Printable acid-modified corn starch as non-toxic, disposable hydrogel-polymer electrolyte in supercapacitors

Andreas Willfahrt, Erich Steiner, Jonas Hoetzel and Xavier Crispin

The original publication is available at www.springerlink.com:
Willfahrt, A., Steiner, E., Hoetzel, J., Crispin, X., (2019), Printable acid-modified corn starch as non-toxic, disposable hydrogel-polymer electrolyte in supercapacitors, *Applied Physics A*, 125(7), 474. https://doi.org/10.1007/s00339-019-2767-6

Original publication available at:
https://doi.org/10.1007/s00339-019-2767-6

Printable Acid Modified Corn Starch as Non-Toxic, Disposable Hydrogel-Polymer Electrolyte in Supercapacitors

Andreas Willfahrt[1,2], Erich Steiner[2], Jonas Hötzel [2], Xavier Crispin[1,3]

[1] Laboratory of Organic Electronics, Department of Science and Technology, Linköping University, SE-60174, Norrköping, Sweden

[2] Innovative Applications of the Printing Technologies, Stuttgart Media University, 70569, Stuttgart, Germany

[3] Wallenberg Wood Science Center, ITN, Linköping University, 602 21 Norrköping, Sweden.

Corresponding author:

Andreas Willfahrt, e-mail: willfahrt@gmail.com, phone: +49 711 9120135

Abstract

Corn starch and citric acid, two low-cost and abundant materials, were used for establishing a novel screen printable hydrogel for printed electronics applications. Corn starch was modified with citric acid by melt-blending, the so obtained thermoplastic starch was ground to powder and added to a water-starch suspension. Ultrasonication was used to prepare hydrogels of different citric acid concentrations. The most promising hydrogel contained 10 % citric acid by weight, provided an ionic conductivity of (2.30 ± 0.07) mS·cm^{-1} and appropriate rheological properties for screen and stencil printing. The hydrogel shows superb printability and prolonged stability against degradation. The corn starch hydrogel was used as printable gel polymer electrolyte in fully printed supercapacitors. The specific capacitance of the printed supercapacitor reached 54 F·g^{-1}. The printable hydrogel polymer electrolyte is easy to produce without in-depth chemical knowledge, is based on widely used and non-toxic materials and may be used as a functional layer in other printed electronics applications such as printed batteries.

Keywords: screen and stencil printing, gel polymer electrolyte, supercapacitor, printed electronics, energy storage

1 Introduction

The terms Internet of Things (IoT), Internet of Everything (IoE) are referred to the use of internet to connect things with each other and to people. This implies that electronic circuits and antenna are functionalising things. IoT allows for the automation of more and more tasks [1]. This approach of making everything smart requires an inconceivable number of sensors and actuators, which must be powered by the power grid or by mobile power sources if no connection to the grid is available [2]. Energy generating devices such as thermoelectric or piezoelectric converters can supply these sensors with power. However, these energy harvesters usually deliver only intermittently and do not deliver sufficient power [3]. One solution is to use printed energy storage devices as energy buffers between the harvester and the wireless sensor circuits. The harvesting device charges a battery or supercapacitor in order to deliver higher peak power to the sensor circuit.

The functionalisation of things with sensors, electronic circuits and energy devices requires to physically putting electronic tags on physical objects. In that context, the traditional manufacturing technique for the electronics and energy devices must be revised to enable the mass production of devices at ultra-low cost and possibility for completely new form factors. Printed electronics is explored as promising manufacturing method to integrate electronics to things/objects because it could deliver low unit costs and very high unit numbers. Yet another key aspect is the impact of electronics on every things and the issue of recyclability and environmental impact. If possible, only materials that are harmless to the environment should be used, because the service life of printed electronic devices is finite and environmentally friendly disposal of these devices must be ensured.

Supercapacitor is the generic term for electric double layer capacitors (EDLC), pseudocapacitors and hybrid capacitors. Pseudocapacitors are based on faradaic processes that do not occur in EDLC where charges accumulate on the electrode

surfaces. The combination of both is called hybrid supercapacitor [4, 5] or supercapattery [6]. Independent of supercapacitor type, printing is a feasible manufacturing method, either by using a co-planar or a stacked multilayer design [7, 8]. The simplest stacked multilayer design consists of two current collectors, two electrode layers and a separator soaked with electrolyte. The most important properties of the electrodes include high conductivity and surface area. Paste of silver particles is frequently used to print conducting layer that can be used as collector in a supercapacitor. It may be contrary to common sense to use the precious metal silver in disposable products. However, a scientific study on this subject showed that silver particle residues were not rated as hazardous waste [9]. The separator should enable the ions of the electrolyte to move as freely as possible. Separators may be categorised into two types: nonwovens and solid electrolytes. The latter can be applied e.g. in printing processes. In nonwovens, a three-dimensional network of fibres is created depending on the employed manufacturing process [10]. Due to high ion mobility, polymeric nonwovens are frequently used in electrochemical storage devices. In printed electronics, solution processable electrolytes are favourable, since a fully printed device is easier to produce. Thus, gel polymer electrolytes are addressed by researchers [11, 12], although the ion conductivity is lower compared to the nonwoven separator type. There are different approaches to realise printable gel polymer electrolytes. Natural starting materials such as polysaccharides are ideal for the goal of developing an environmentally compatible gel polymer electrolyte (GPE). Recently published articles show that this field is of interest.

Ma et al. [13] prepared solid polymer electrolytes by melt extrusion of starch with glycerol and added electrolyte salt (LiCl, NaCl, and KCl). They found that salt concentration affects conductivity, but water content has higher impact. Railanmaa et al. [14] also used NaCl in physically cross-linked wheatstarch and gelatine hydrogels that yielded high ionic conductivity. Lin et al. [15] reported on a solid polymer electrolytes in lithium sulphur batteries. Food grade corn starch dissolved in dimethyl sulfoxide (DMSO) with silane additive was doped with lithium bis-(trifluoromethanesulfonyl)imide (LiTFSI). Ramesh et al. [16] used LiTFSI and an ionic liquid, which increased the amorphous character and thus ionic conductivity of corn starch. Ammonium nitrate (NH_4NO_3) and ammonium bromide (NH_4Br) was used by Khiar et al. [17] as well as by

Shukur and Kadir [18]. The maximum conductivity was obtained by NH_4NO_3 concentration of 25 wt%.

Hydrogels are polymer networks that are able to incorporate a huge amount of water in the polymer-matrix. This absorption may be accompanied by a massive increase in volume [19]. The majority of hydrogels increase their volume by water retention, thus leading to a more amorphous inner gel structure. An interesting class of hydrogels is based on polysaccharides such as the abundant corn starch [20]. Starch is a white, tasteless and odourless powder that is insoluble in cold water or alcohol. The physical modification, i.e. the gelatinisation of corn starch, can simply be carried out by heating a starch-water suspension to approx. 85 °C. Native starch occurs naturally in the form of insoluble, semi-crystalline granules, which are made up of two types of molecules: the linear and helical amylose and the branched amylopectin. Depending on the plant, starch generally contains 20 to 25 % amylose and 75 to 80 % amylopectin by weight [21]. As shown in Figure 1, amylopectin contains polymer chains with up to 10,000 D-glucose units, linked by α-1,4-glycosidic bonds. Every 24 to 30 units branching takes place by α-1,6-glycosidic bonds. Amylose is composed of continuous, unbranched chains forming a helix with as many as 4,000 D-glucose units. The glucose-units are also linked by α-1,4-glycosidic bonds [22]. Carboxylic acids, such as citric acid, are multifunctional reactants that can be used e.g. for crosslinking starch [23], plasticising [24] and compatibilising [25] purpose. Although many commodity applications include polysaccharides, hydrogel based on corn starch has never been investigated for creating a green, printable electrolyte layer for energy storage application.

In this work, we examine new printable GPE based on corn starch and citric acid (CA) to ensure high natural abundance, absence of toxicity and biodegradability. The CA has two functions, that of the crosslinking agent and the electrolyte. We characterise the blends, the rheological properties, and the ionic transport and integrate such layers by printing technologies in a supercapacitor structure. The investigated supercapacitors are characterised by non-toxic materials and simple and robust design. The supercapacitors can act as energy storage on disposable packaging material and consist mainly of biodegradable materials.

2 Experimental procedure

2.1 Preparation of Citric Acid Modified Hydrogels

Native corn starch (ST) was bought at the grocery store. The moisture meters Sartorius MA30 and Kern MLB 50-3 were used for measuring the humidity of the native ST, which is between 10-15 % RH at room temperature. Anhydrous citric acid (CA) was bought from Carl Roth chemicals (Karlsruhe, Germany). Activated carbon powder Norit A SUPRA EUR and conductive carbon-black VXC72R was donated by Cabot GmbH (Rheinfelden, Germany). PEDOT:PSS PH1000 was sponsored by Heraeus (Hanau, Germany).

CA powder was molten on a laboratory hot plate Heidolph MR Hei-Tec (Schwabach, Germany) at 160 °C. ST powder was added to the molten CA in a ratio (wt/wt) of 1:1 and 1:4 (ST:CA). The obtained thermoplastic starch (TPS) was then ground to powder and later on used as an additive in the process of preparing hydrogels.

The hydrogels were prepared as follows: dry TPS powder and D.I. water were added to the mixing container and stirred for few seconds using an ultrasound processor Hielscher UP200Ht Processor (Teltow, Germany) with a diameter of the sonotrode horn tip of 7 mm. ST was added to the suspension. Afterwards, ultrasound processing was performed with an amplitude of 100 % and a frequency of 26 kHz. The sonotrode horn was immersed into the suspension. The end of gelatinisation was indicated by a drop in the applied power, which was accompanied by a remarkable reduction of processing noise, indicating a sudden increase of viscosity. The process was then stopped immediately. The prepared gel was stored at room temperature (23 °C) in glass vials sealed with parafilm. Indirect ultrasound processing was also tested, as reported by Herceg et al. [26]. However, the so obtained hydrogels showed a different gel structure and lower viscosity. Additionally, the processing time was remarkably longer, so that the direct processing was preferred. The ultrasound treatment leads to increased water absorption in starch [27]. The ultrasonic treatment is a combination of cavitation, i.e. massive shearing, and a temperature increasement caused by shearing to approx. 70 °C, which leads to a close contact between water and starch in order to obtain a homogeneous hydrogel [27–29].

The obtained hydrogel was then printed on a laboratory screen-printing machine.

2.2 Printing Technology

Printing tests were performed with half-automatic screen/stencil printing machine Asys Ekra X1 (Bönnigheim, Germany). The screen meshes PET 1500 77-48, 54-64 and 18-180 were donated by SEFAR (Thal, Switzerland). The photoemulsion KIWOCOL POLY-PLUS SRX was sponsored by Kissel+Wolf (Wiesloch, Germany).

The layout of the printed supercapacitors comprised of four successively printed layers. The current-collectors consisted of silver ink LOCTITE EDAG PM 406 E&C (Düsseldorf, Germany), which were covered by an additional carbon-black (LOCTITE EDAG PF 407C E&C) layer for electrochemical passivation. The PET substrate Bleher Optimont 501 (Ditzingen, Germany) was used. The screen printed electrode consisted of activated carbon Cabot Norit A SUPRA EUR, PEDOT:PSS PH1000, carbon-black conductive additive Vulcan VXC72R and purified water, see Table 3. The used amount of water allows adapting the viscosity of the gel to the requirements of the coating process. The electrode layer was printed with 54-64 and 18-180 screen mesh, resulting in 50 or 150 µm layer thickness respectively. The hydrogel can be applied by screen and stencil printing. Stencil printing is advisable, if the adhesion of the electrodes is limited, so that ink splitting may pull of the previously printed electrode layer from the substrate. Since the adhesion of the screen printed electrode layer is not very pronounced, the hydrogel polymer electrolyte was applied by means of stencil printing.

2.3 Characterisation

The thermoplastic starch powders obtained by melt-blending CA and ST were characterised using differential scanning calorimetry (DSC) and Fourier-transform infrared spectroscopy (FTIR). DSC analysis was performed with Netzsch DSC 204 Phoenix (Selb, Germany) with autoloader unit. All measurements were obtained under nitrogen atmosphere. The samples were examined in hermetic sample pans. The starting temperature was 25 °C and it was raised to 180 °C at a scan rate of 5 K/min. Data analysis was performed with Proteus software.

FTIR measurements were performed with Nicolet i10s (ThermoFisher Scientific, USA) including an attenuated total reflection (ATR) unit, which allows measurements of powders, gels, and liquids. The spectra were obtained by average of 32 scans from 700 to 4000 cm^{-1}. Spectragryph Software was used for data processing.

The rheological properties of the hydrogels were characterised using an Anton Paar MCR300 Rheometer (Ostfildern, Germany). A cone-plate system (CP25-1) with a

diameter of 25 mm and a cone angle of 1° at 50 µm measurement gap was deployed. The temperature control unit TEK 150P was held at 23 °C. Data was analysed using Rheoplus Software.

The gel polymer electrolyte was used in fully printed supercapacitors, which were characterised by electrochemical techniques. Cyclic voltammetry (CV) and galvanostatic charge-discharge (GCD) measurements were performed with biologic BCS-805 battery cycling system (Seyssinet-Pariset, France). The ionic conductivity of the hydrogels was measured with the biologic SP-300 potentiostat providing a maximum frequency of 7 MHz with a voltage amplitude of 10 mV at room temperature. EC-Lab Software allows for data processing and data fitting.

3 Results and Discussion

3.1 Differential Scanning Calorimetry (DSC) of Thermoplastic Starch (TPS)

The TPS powder made from starch and citric acid (see section 2.1) was characterised by differential scanning calorimetry (DSC) and compared with pure CA. Melting point depression is illustrated in Figure 2. We observe an increase in melting temperature with increasing amount of CA with a very broad peak at 135 °C for 1:1 mixing ratio, a peak at 145 °C for 4:1 ratio and a narrow peak at 160 °C for pure CA. Low onset temperature T_o is associated with the amorphous character of the melt-blended acid/starch mixture. Higher enthalpies and melting temperatures indicate a higher degree of crystallinity of the granules, probably due to unreacted acid [30]. Due to the lower onset temperature, the mixing ratio of one part CA and one part ST was used in the further course of this work.

3.2. Preparation of the hydrogel and cross-linking.

Due to the fact that it was not possible to obtain stable hydrogels with solely TPS and water, ST was added to facilitate the process. The hydrogels were thus prepared through a second step by mixing TPS powder, D.I. water and ST under ultrasound sonication. Upon ultrasound treatment or heating in presence of excess water, native starch granules swell, partially disintegrate as a result of microscopic changes related to the dissociation of the double helices and melting of crystallites and escape of polysaccharides [31]. These events take place upon the so-called gelatinisation

characterized by a dramatic change in granule morphology leading to gel formation [32]. Note that the presence of CA also modifies the gel formation. Indeed, citric acid is a tri-carboxylic acid used to cross-link the polysaccharide molecules with each other. We introduce CA to control the viscosity, the rheology of the GPE, but also to introduce protons to promote ionic conductivity. See detailed description of the hydrogel preparation in section 1 of the supplementary information.

The chemical reaction of CA and ST is depicted in Figure 3 as proposed in several publications [33–36].

Microscope images of dry hydrogel layers obtained with low content of CA 5 wt% (a) and 10 wt% (b) in Figure 4 display a highly swollen, amorphous and granular structure. In contrast, with a high content in CA (25 wt% and 20 wt%) only a few amorphous gel structures are visible and the gel becomes more homogenous likely because of the high content in citric acid and the consequent acid hydrolysis which depolymerizes the starch molecules into smaller polysaccharides and promote the destruction of the starch granules. A more detailed optical analysis of the dry hydrogel layers is presented in the supplementary information section 4.

3.2 Rheological Properties of Hydrogels for Screen Printing

Screen printing is a very convenient process that allows the use of liquids of different viscosities. Gaikwad et al. [37] report the possibility to use a viscosity range of 100 to 100 000 mPa·s for screen printing. The rheological properties of printing inks, such as viscosity and thixotropy, do not only influence processability, but also other properties such as ink film thickness, surface structure and edge quality of the printed image. To evaluate the shelf life of the gels or the stability of the ink, the gel viscosity is monitored over a certain period of time. A medium shear rate of 100 s^{-1} was chosen for rotational viscosity determination. For more information on rheological measurements see supplementary information section 3.

The CA concentration in the hydrogel is varied by adding different weight percent (wt%) of thermoplastic starch powder to the H_2O-ST mixture. Since the used TPS powder contains the same amount of CA and ST, the amount of ST in the H_2O-ST suspension was adjusted in order to keep it constant at 30 wt%, see Table 1. The dynamic viscosities of hydrogels increase with a decreasing content of CA and an increasing content of water,

from 1.7 Pa·S at 25wt% of CA to 20 Pa·S at 5wt% of CA. This suggests that crosslinking is established for low wt% CA and when an excess of CA is introduced in the gel, the viscosity gets lower because a large fraction of CA is not cross-linked and is soluble in water. Moreover, the large amount of CA leads to an efficient hydrolysis of the polysaccharide into small molecular weight chains accompanied with the disintegration of the starch granules during gelation. Hence, high CA content leads to low a viscosity gel electrolyte.

With the lowest CA concentration of 5 % by weight, a hydrogel is obtained that is very similar to the physically modified hydrogel without CA. After only three days, this gel shows a clear change in texture with a tendency to lump formation. The hydrogels with a higher CA content than 10 % by weight are low viscosity liquids with a weak gel character. In the gelatinisation of the latter variants, the ultrasound treatment is not stopped when the energy drops, but when bubbles form in the fluid, as no such increase in viscosity can be observed as with the other samples. Both samples resemble stickier liquids more than gels, so that different print parameters are required than with pronounced gel character, such as the gel with 10 wt% CA.

3.3 FTIR Measurements of the Hydrogels

The FTIR spectra of CA modified hydrogels made of TPS and water-starch suspension are shown in Figure 5.

There are characteristic peaks at 1715 cm^{-1}, 1636 cm^{-1}, 1208 cm^{-1}, and 1020 cm^{-1}, see Table 2. The peak 1020 cm^{-1} is typical of C-O stretching within the glucose-based ring; while the two contributions at 1715 cm^{-1} and ~1200 cm^{-1} are specific to the protonated form of the carboxylic acid group (-COOH) present in citric acid, corresponding to the C=O stretching ($\nu_{C=O}$) and the C-OH combined mode of stretching and bending (ν_{C-OH}), see Figure 6. The two other peaks at 1636 cm^{-1} and ~1400 cm^{-1} are specific to the deprotonated, i.e. the carboxylate form ($-COO^-$), as it was illustrated in the literature for both monocarboxylate [38] and dicarboxylate [39]. While strong acids ionise essentially completely in water and the percent ionisation is always approximately 100%, regardless of the concentration; it is not the same situation for weak carboxylic acid groups like those in CA. In that case, the percent ionisation in solutions is small and depends on the concentration of CA. The percent ionisation of a

weak acid increase as its analytical concentration decreases. It therefore means that at a low concentration of CA in the gels, the ionised carboxylate form (COO^-) is predominant, while when we increase the concentration of CA, the protonated form becomes dominant. This explains why for 5 wt% and 10 wt% CA in the gel, the carboxylate contribution at 1636 cm^{-1} increases, but further increasing the CA concentration leads to a decrease of that vibration 1636 cm^{-1}; but an increase of the carbonyl stretching of the protonated form at 1715 cm^{-1}. Note that even not shown in the figure, we observe an increasing 0-H stretching of water at ~3400 cm^{-1} for a decreasing amount of CA as indicated by the composition in Table 1. Additional results of FTIR analysis of the starting materials can be found in supplementary information section 2.

Based on the analysis results of the tested hydrogel formulations, the mixture with 10 wt% CA content is the most appropriate screen and stencil printable hydrogel electrolyte providing reasonable ionic conductivity and appropriate rheological properties. Accordingly, all examined supercapacitors were produced with this hydrogel.

3.4 Ionic Conductivity Measurements

The ionic conductivity of the solid electrolyte determines one important resistive component of the internal resistance of the supercapacitor and it can affect the achievable effective specific capacitance of the supercapacitor obtained at different charge rates [40]. Here, we determine ionic conductivity by electrochemical impedance spectroscopy [14] and investigate the effect of the CA concentration in the GPE. When the phase angle of the impedance is zero, the impedance has a pure resistive component and provides the value of the resistance *R*. The conductivity is calculated by $\sigma = l/(R \cdot A)$ with *σ, l, R* and *A* representing the electrical conductivity, the length or thickness, the resistance and the cross-sectional area of the conductor. See section 6.1 in the supplementary information for a detailed description.

Repeated measurements with hydrogel layers of different thicknesses (100, 360, 750 and 1000 µm) have always shown the same tendency: the highest ionic conductivity is achieved at a CA concentration of 10% by weight; while the highest CA concentration leads to the lowest ionic conductivity. In order to explain the maximum of conductivity for 10 wt% CA, it is necessary to remind that the ionic conductivity is directly

proportional to the concentration of dissociated ions and the diffusion coefficient *D* of those ions. We assume that the ionic conductivity is dominated by the proton conductivity in water since the carboxylate molecule is attached on the rather large anions of the CA or immobilised by crosslinking to the polysaccharide. Hence, the Grotthuss-type mechanism for protons is likely dominant as in other aqueous acidic liquids [41]. This mechanism assumes that the protons themselves do not move, but the charge transport takes place via displacing the proton through hydrogen bonding. Since CA is a weak acid, the concentration of dissociated ions (carboxylate and proton) will vary with the concentration of CA in the gel. This is indeed what we found with the FTIR analysis: the 10 wt% CA has the highest concentration in dissociated carboxylate form and thus the highest concentration in mobile protons; while at higher concentration of CA the number of dissociated ions is less. We believe that this is the major effect that explains the maximum of the ionic concentration for 10 wt% CA. Note however that another effect also come into play. This is the variation of the diffusion coefficient of the ions with the viscosity of the gel. Indeed, the large amount of CA leads to a low viscosity gel electrolyte (see section 3.2); which would favour ionic diffusion and transport. Indeed, the Stokes – Einstein model connects directly the diffusion coefficient and the viscosity of the medium: $D = kT/6\pi r_H \eta$; where, k is the Boltzmann constant, T is the absolute temperature, η is the viscosity of the medium, and r_H is the hydrodynamic radius of the proton.

3.5 Supercapacitor Properties

The layout of the printed supercapacitors comprised of four successively printed layers is displayed in Figure 7. The current-collectors consisted of silver ink printed on PET substrate. The silver contact was then covered by an additional carbon-black layer for electrochemical passivation. The electrode made of activated carbon, carbon-black conductive additive and conductive polymer PEDOT:PSS was screen printed on top of this. The electrode layer was about 50 or 150 µm in thickness depending on the printing mesh and its formulation is summarised in Table 3.

The ST-CA hydrogel can be applied by screen and stencil printing with adjustable thickness as well. The hydrogel containing 10 wt% CA is chosen because of its highest ionic conductivity and its decent viscosity for printing. This natural polymer gel

electrolyte played both the role of the electrolyte and the separator layer in the supercapacitor. The geometrical area of the electrodes in the supercapacitor was 10 cm^2. After all layers have been printed, the two electrodes are assembled on top of each other and glued, see also supplementary information section 5.

The specific capacitance C_{sp} was determined by galvanostatic charge and discharge (GCD) technique at different charge/discharge currents. EIS measurements were carried out on certain samples as a crosscheck for equivalent serial resistance (ESR) and capacitance. The comparison of C_{sp} and ESR values determined by CV, GCD and EIS provides adequate results.

The charge and discharge capacitances are calculated from galvanostatic cycling with potential limitation (GCPL), according to $C = Q_{ch/disch}/\Delta E_{WE}$ where $Q_{ch/disch}$ is the total charge stored or released by the supercapacitor. ΔE_{WE} is the difference between the initial and final potential on either charging or discharging process. When symmetric supercapacitors are characterised, division of capacitance C by the mass of one electrode m results in the specific capacitance C_{sp} in $F \cdot g^{-1}$. When printing supercapacitor structures, the relationship between the surface of the capacitor and the capacitance is also considered. In this case, the capacitance C is referenced to the area of the electrodes A instead of the mass m.

The specimens with the separator made of the CA modified hydrogel achieved C_{sp} of around 20-36 $F \cdot g^{-1}$ and showed reasonable low leakage-current indicated the small slope in the plateau-region of the CV curves at 25 $mV \cdot s^{-1}$ illustrated in Figure 8 (a). The galvanostatic charge-discharge response is shown in Figure 8 (b), indicating a stable supercapacitor. The voltage of the supercapacitor follows a quasi-triangular shape, which is a desired behaviour with low ESR. In Figure 8 (c) the current density is shown, which is between 90 and 220 $A \cdot g^{-1}$.

The areal specific capacitance is shown in Figure 9 (a). The hydrogel containing 10 wt% CA performs better than the other formulations, achieving an areal capacitance of 279 $mF \cdot cm^{-2}$ at a discharge current of 1 mA. This result maybe deduced from the ionic conductivity, which was highest with 10 wt% CA fraction.

In order to evaluate the results of the starch-based GPE, supercapacitors with nonwoven separators soaked with CA solution were also characterised. Specific

capacitances with both separator types are similar. However, with printed hydrogel separators the decrease in specific capacitance is lower as the discharge current increases, as shown in Figure 9 (b).

The hydrogel separator is in intimate contact with the electrodes, so that even deep pores may be penetrated by the GPE. As such, the hydrogel separator quickly offers more locations for the accumulation of charge carriers. With nonwovens, the contact is less intimate, so that a greater effect can be seen due to the longer charging time, i.e. voltage hold at maximum voltage, than with the hydrogel separator. Thereby it is possible to arrange a higher amount of charge on the electrode surface. The constant voltage step between constant current charging and discharging increases the capacitance, as the ions can also penetrate deep pores and thus generate a higher charge on the electrodes.

Repeated tests with various electrode formulations and layer thicknesses did not increase C_{sp} above 36 $F \cdot g^{-1}$. It was assumed that this limit was due to the concentration of hydronium ions of the dissociated CA. The addition of further CA solution shifted this upper limit so that specific capacitance was increased by 40-46 %.

This increase is not linear as the capacitance decreased with further increased volume of CA solution, as shown in Figure 9 (c). We hypothesised that by adding more CA solution, the viscosity of the GPE decreases. This may promote detachment of the electrode, which only weakly adheres to the current collector due to low binder content. Additionally, as discussed earlier, excess CA may lead to ion aggregation and ion pairs, so that the number of free ions is reduced.

Table 4 shows the characteristic values of printed supercapacitors published elsewhere. The results obtained with the novel corn starch-based hydrogel are promising and show that it is very well suited as a solid hydrogel electrolyte for fully printed supercapacitors.

4 Conclusion

Thermoplastic starch obtained by melt-blending CA with ST was used as additive for screen printable gel polymer electrolyte. The hydrogels with different concentrations of the thermoplastic starch powder indicate a broad spectrum of rheological and electrochemical properties as well as good resistance to mould growth and retrogradation with a significantly longer pot life than the physically cross-linked corn

starch hydrogel. It was found that the hydrogel with 10 wt% CA is best suited for screen printing of functional layers, e.g. gel polymer electrolyte in printed batteries or supercapacitors. The corn starch-based gel polymer electrolyte achieved comparable characteristics to printed supercapacitors reported elsewhere. CA serves a dual function as modifier of ST and as electrolyte in the separator layer of the supercapacitor. The completely printed supercapacitors are made completely of non-toxic materials and achieved a specific capacitance in the range of around 35 $F \cdot g^{-1}$ or 279 $mF \cdot cm^{-2}$ without additional electrolyte. With an increased potential window of 1.2 V and an additional constant voltage step prior to discharge at constant current, the specific gravimetric capacitance was increased to 54 $F \cdot g^{-1}$.

5 Acknowledgements

The authors acknowledge financial support from the Swedish Government Strategic Research Area in Materials Science on Functional Materials at Linköping University (Faculty Grant SFO Mat LiU No. 2009 00971), Knut and Alice Wallenberg Foundation, the Swedish Foundation for Strategic Research, VINNOVA (Digital Cellulose Center) and the Swedish Research Council.

6 References

1. S. Ornes, Proceedings of the National Academy of Sciences of the United States of America (2016) doi:10.1073/pnas.1613921113
2. M.H. Miraz, M. Ali, P.S. Excell, R. Picking, in *2015 Internet Technologies and Applications (ITA),* Wrexham, United Kingdom, p. 219
3. F.K. Shaikh, S. Zeadally, Renewable and Sustainable Energy Reviews (2016) doi:10.1016/j.rser.2015.11.010
4. J.H. Kim, H.J. Choi, H.-K. Kim, S.-H. Lee, Y.-H. Lee, International Journal of Hydrogen Energy (2016) doi:10.1016/j.ijhydene.2016.06.018
5. H. Omidian, J.G. Rocca, K. Park, Macromolecular bioscience (2006) doi:10.1002/mabi.200600062
6. G.Z. Chen, International Materials Reviews (2016) doi:10.1080/09506608.2016.1240914
7. A. Leela Mohana Reddy, F. Estaline Amitha, I. Jafri, S. Ramaprabhu, Nanoscale Res Lett (2008) doi:10.1007/s11671-008-9127-3
8. L. Sun, X. Wang, W. Liu, K. Zhang, J. Zou, Q. Zhang, Journal of Power Sources (2016) doi:10.1016/j.jpowsour.2016.03.019
9. James Edward Atkinson, Doctoral Thesis, Western Michigan University, Juni 2017, https://scholarworks.wmich.edu/dissertations/3144/. Accessed 27 July 2018
10. P. Kritzer, J.A. Cook, J. Electrochem. Soc. (2007) doi:10.1149/1.2711064
11. L. Boonen, P. Kitzler, J. Kasum, Progress in Organic Coatings (2018) doi:10.1016/j.porgcoat.2017.10.006
12. S. Lawes, A. Riese, Q. Sun, N. Cheng, X. Sun, Carbon (2015) doi:10.1016/j.carbon.2015.04.008
13. X. Ma, J. Yu, K. He, Macromol. Mater. Eng. (2006) doi:10.1002/mame.200600261
14. A. Railanmaa, S. Lehtimäki, D. Lupo, Appl. Phys. A (2017) doi:10.1007/s00339-017-1068-1
15. Y. Lin, J. Li, K. Liu, Y. Liu, J. Liu, X. Wang, Green Chem. (2016) doi:10.1039/c6gc00444j
16. S. Ramesh, R. Shanti, E. Morris, R. Durairaj, Materials Research Innovations (2013) doi:10.1179/143307511X13031890747291
17. A.S.A. Khiar, A.K. Arof, Ionics (2010) doi:10.1007/s11581-009-0356-y
18. M.F. Shukur, M.F.Z. Kadir, Ionics (2015) doi:10.1007/s11581-014-1157-5

19. C. Demitri, R. Del Sole, F. Scalera, A. Sannino, G. Vasapollo, A. Maffezzoli, L. Ambrosio, L. Nicolais, J. Appl. Polym. Sci. (2008) doi:10.1002/app.28660
20. H. Ismail, M. Irani, Z. Ahmad, International Journal of Polymeric Materials and Polymeric Biomaterials (2013) doi:10.1080/00914037.2012.719141
21. Kuokkanen (M.), Vilppo (T.), Kuokkanen (T.), Stoo (T.), Niinimaki (J.), BioResources Journal **4**, 4331 (2011)
22. W.H. Brown, T. Poon, *Introduction to Organic Chemistry,* 5th edn. (John Wiley & Sons, Inc.2012)
23. N. Reddy, Y. Yang, Food Chemistry (2010) doi:10.1016/j.foodchem.2009.05.050
24. L.C.d. Cruz, C.S.d. Miranda, W.J.d. Santos, A.P.B. Gonçalves, J.C.d. Oliveira, N.M. José, Mat. Res. (2015) doi:10.1590/1516-1439.370814
25. J.B. Olivato, M.V.E. Grossmann, F. Yamashita, D. Eiras, L.A. Pessan, Carbohydrate Polymers (2012) doi:10.1016/j.carbpol.2011.11.035
26. I.L. Herceg, A.R. Jambrak, D. Subaric, M. Brncic, S.R. Brncic, M. Badanjak, B. Tripalo, D. Jezek, D. Novotni, Z. Herceg, Czech Journal of Food Sciences **28**, 83 (2010)
27. M. Sujka, J. Jamroz, Food Hydrocolloids (2013) doi:10.1016/j.foodhyd.2012.11.027
28. A. Hu, S. Jiao, J. Zheng, L. Li, Y. Fan, L. Chen, Z. Zhang, LWT - Food Science and Technology (2015) doi:10.1016/j.lwt.2014.10.048
29. A.R. Jambrak, Z. Herceg, D. Šubarić, J. Babić, M. Brnčić, S.R. Brnčić, T. Bosiljkov, D. Čvek, B. Tripalo, J. Gelo, Carbohydrate Polymers (2010) doi:10.1016/j.carbpol.2009.07.051
30. Y. Zhang, J Bioproces Biotechniq (2014) doi:10.4172/2155-9821.1000161
31. S. Wang, L. Copeland, Critical reviews in food science and nutrition (2015) doi:10.1080/10408398.2012.684551
32. J. Maitra, V.K. Shukla, American Journal of Polymer Science **4**, 25 (2014)
33. A. Uliniuc, T. Hamaide, M. Popa, S. Băcăiță, Soft Materials (2013) doi:10.1080/1539445X.2012.710698
34. M.A. Osorio, D. Restrepo, J.A. Velásquez-Cock, R.O. Zuluaga, U. Montoya, O. Rojas, P.F. Gañán, D. Marin, C.I. Castro, Journal of the Brazilian Chemical Society (2014) doi:10.5935/0103-5053.20140146
35. A.W.M. Kahar, H. Ismail, N. Othman, J. Appl. Polym. Sci. (2012) doi:10.1002/app.35057

36. P. Nagaraj, A. Sasidharan, V. David, A. Sambandam, Polymers (2017) doi:10.3390/polym9120667
37. A.M. Gaikwad, A.C. Arias, D.A. Steingart, Energy Technology (2015) doi:10.1002/ente.201402182
38. S.E. Cabaniss, I.F. McVey, Spectrochimica Acta Part A: Molecular and Biomolecular Spectroscopy (1995) doi:10.1016/0584-8539(95)01479-9
39. S.E. Cabaniss, J.A. Leenheer, I.F. McVey, Spectrochimica Acta Part A: Molecular and Biomolecular Spectroscopy (1998) doi:10.1016/S1386-1425(97)00258-8
40. G. Wee, O. Larsson, M. Srinivasan, M. Berggren, X. Crispin, S. Mhaisalkar, Adv. Funct. Mater. (2010) doi:10.1002/adfm.201001096
41. M.D.A. Selvakumar, D.K. Bhat, *Biopolymer Electrolytes* (Elsevier, San Diego, 2018)
42. Z. Tehrani, D.J. Thomas, T. Korochkina, C.O. Phillips, D. Lupo, S. Lehtimäki, J. O'Mahony, D.T. Gethin, Energy (2017) doi:10.1016/j.energy.2016.11.019
43. Y. Ling Li, Int. J. Electrochem. Sci. (2017) doi:10.20964/2017.11.32
44. S. Lehtimäki, A. Railanmaa, J. Keskinen, M. Kujala, S. Tuukkanen, D. Lupo, Scientific reports (2017) doi:10.1038/srep46001
45. J.S. Sagu, N. York, D. Southee, K.G.U. Wijayantha, Circuit World (2015) doi:10.1108/CW-01-2015-0004
46. S. Yong, J.R. Owen, M.J. Tudor, S.P. Beeby, J. Phys.: Conf. Ser. (2015) doi:10.1088/1742-6596/660/1/012074
47. S. Lehtimäki, M. Li, J. Salomaa, J. Pörhönen, A. Kalanti, S. Tuukkanen, P. Heljo, K. Halonen, D. Lupo, International Journal of Electrical Power & Energy Systems (2014) doi:10.1016/j.ijepes.2014.01.004

Figure captions

Figure 1: Chemical structure of the corn starch constituting natural polymers amylopectin and amylose. Amylopectin is a branched polymer whereas amylose is a linear polymer forming a helix.

Figure 2: DSC diagram of pure citric acid powder and citric acid (CA) mixed with corn starch in the gravimetric (wt/wt) mixing ratio 1:1 (CAST 1:1) and 4:1 (CAST 4:1).

Figure 3: Cross-linking of citric acid and corn starch.

Figure 4: Optical analysis of dry hydrogel layers. a – d: Order of CA concentration 5, 10, 20, and 25 wt%.

Figure 5: FTIR spectra of hydrogels containing different concentrations of citric acid, whereas the amount of corn starch is constant. The spectra are normalised by the absorbance peak of the characteristic starch band at around 1020 cm^{-1}.

Figure 6: From left to right – illustration of C=O stretching ($\nu_{C=O}$), asymmetric (ν_{as}) and symmetric (ν_{s}) vibrational stretching, and the C-OH combined mode of stretching and bending (ν_{C-OH}).

Figure 7: Schematic illustration of the printed supercapacitor arrangement with current collector (1), electrodes (2), separator and electrolyte (3) and adhesive (4).

Figure 8: (a) Cyclic voltammogram of supercapacitor sample with CA modified hydrogel separator. (b) Full charge/discharge cycle at different currents as obtained by hydrogel separator. (c) Current density and specific capacitance of supercapacitor with CA modified hydrogel separator.

Figure 9: (a) Areal capacitance of hydrogels with different fractions of citric acid. (b) Printed and nonwoven separators. The latter was soaked with one-molar CA solution. (c) Impact of additional CA solution added to the printed hydrogel layer on the specific capacitance.

Figure01

amylopectin

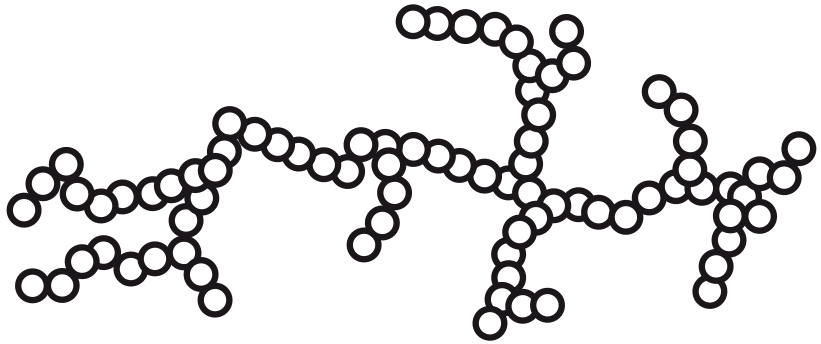

α-1,4-glycosidic bonds

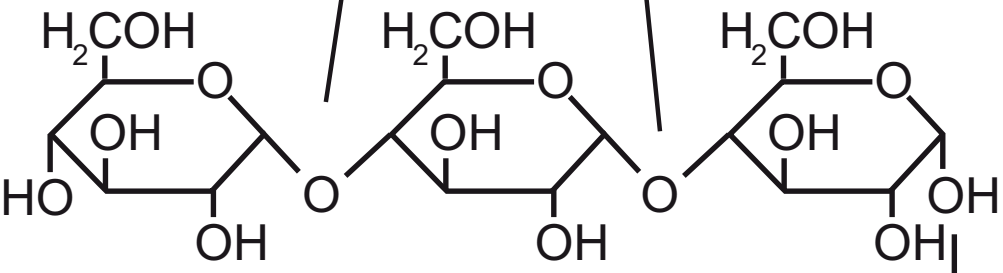

α-1,6-glycosidic bond

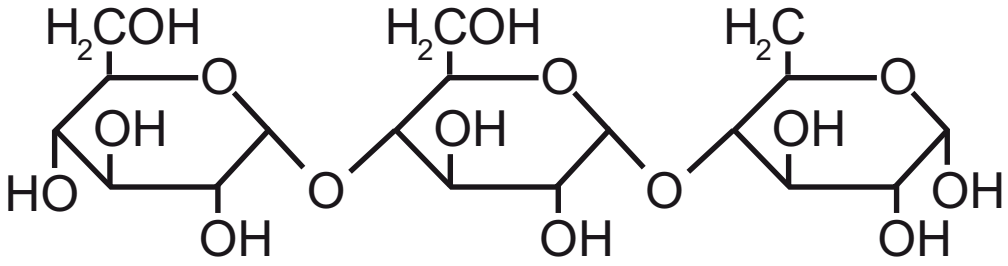

amylose

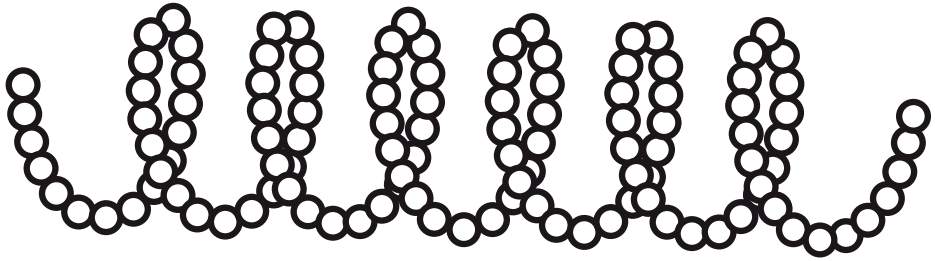

O = single glucose unit

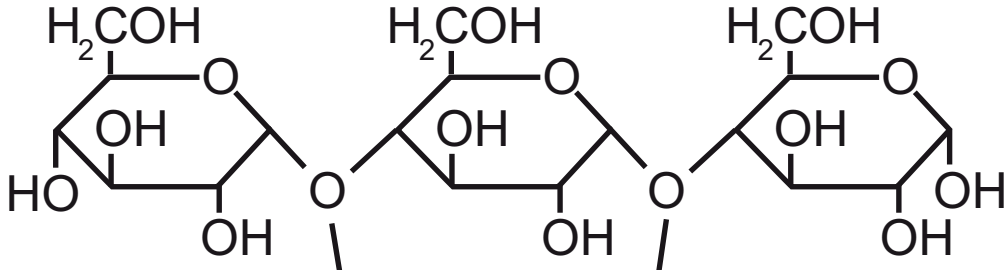

α-1,4-glycosidic bonds

Figure02

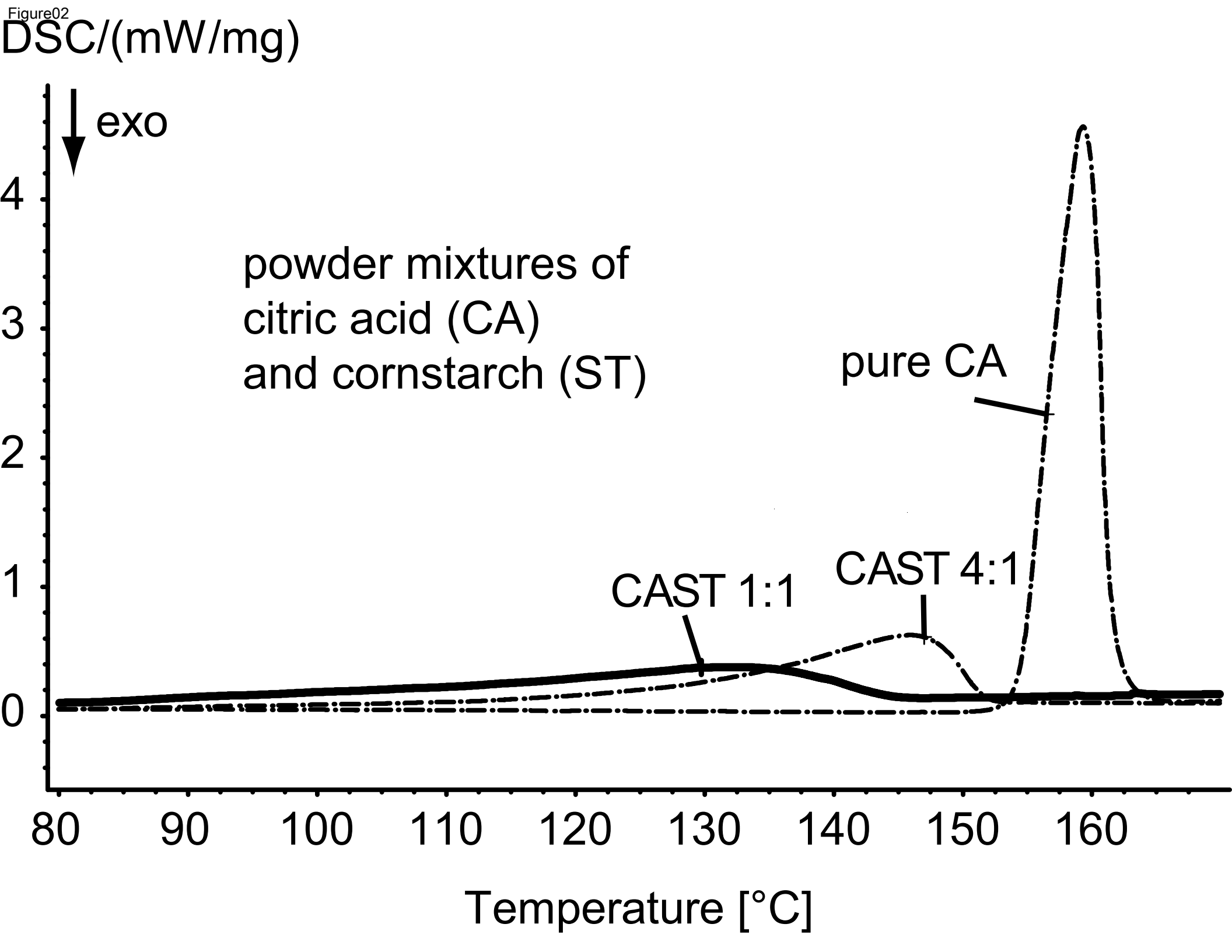
DSC/(mW/mg)
exo
4
3
2
1
0
powder mixtures of
citric acid (CA)
and cornstarch (ST)
pure CA
CAST 1:1
CAST 4:1
80
90
100
110
120
130
140
150
160
Temperature [°C]

Figure03

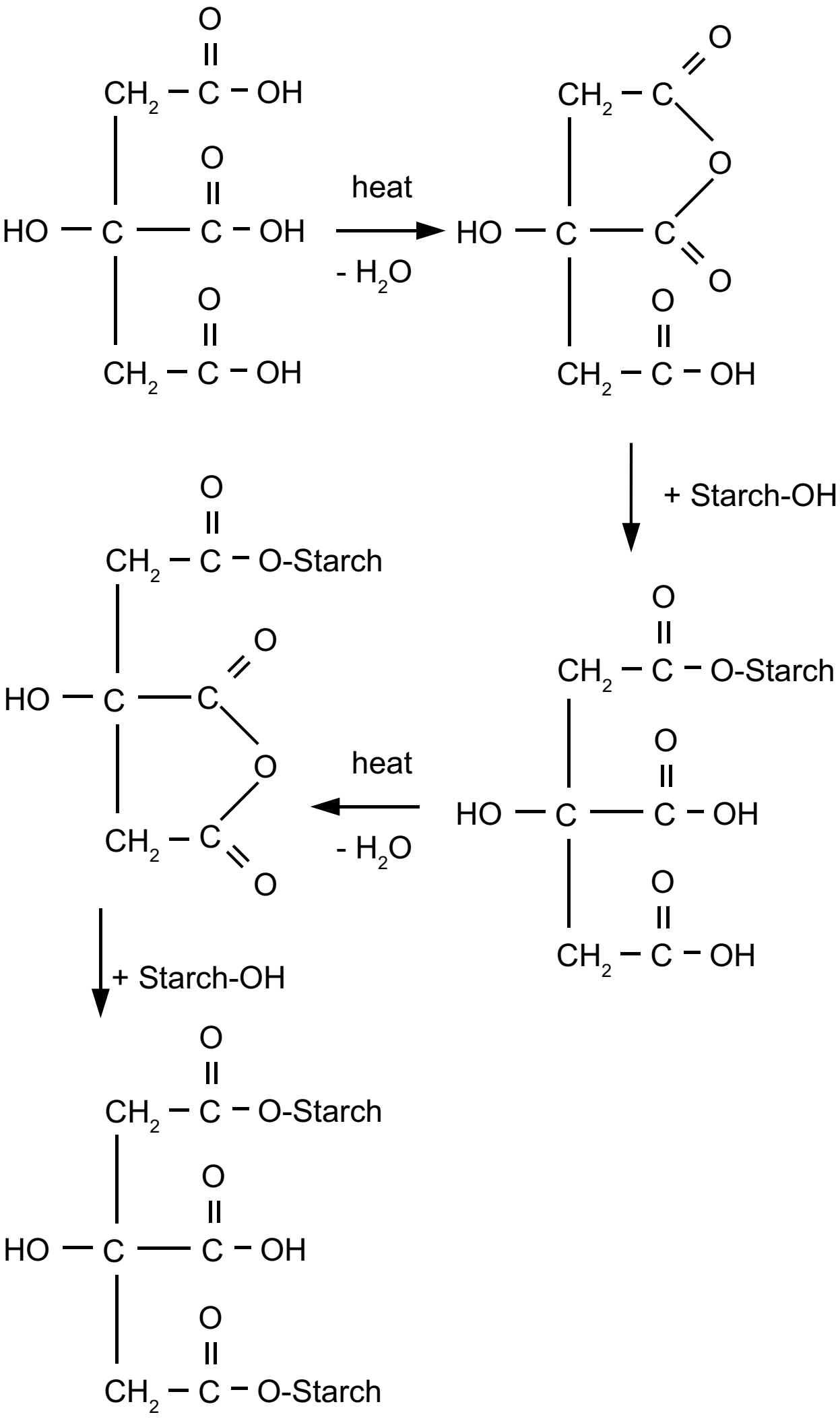

Figure04

Click here to access/download;Figure;Fig04.tif

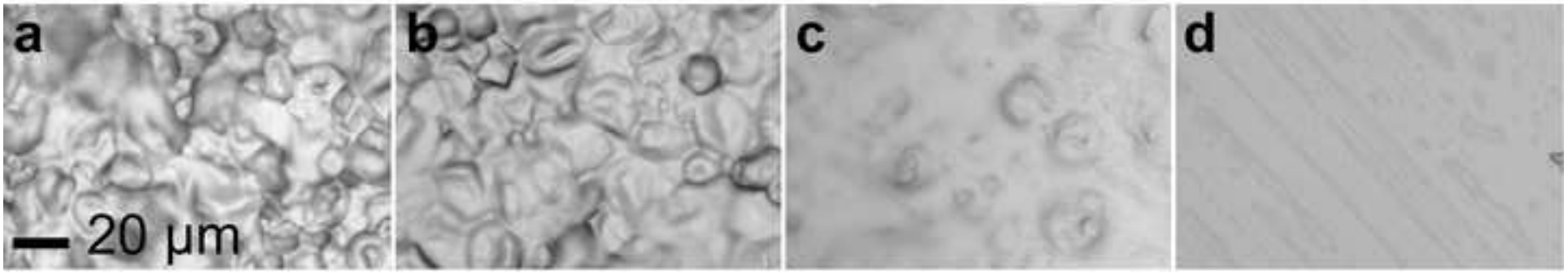

Figure05

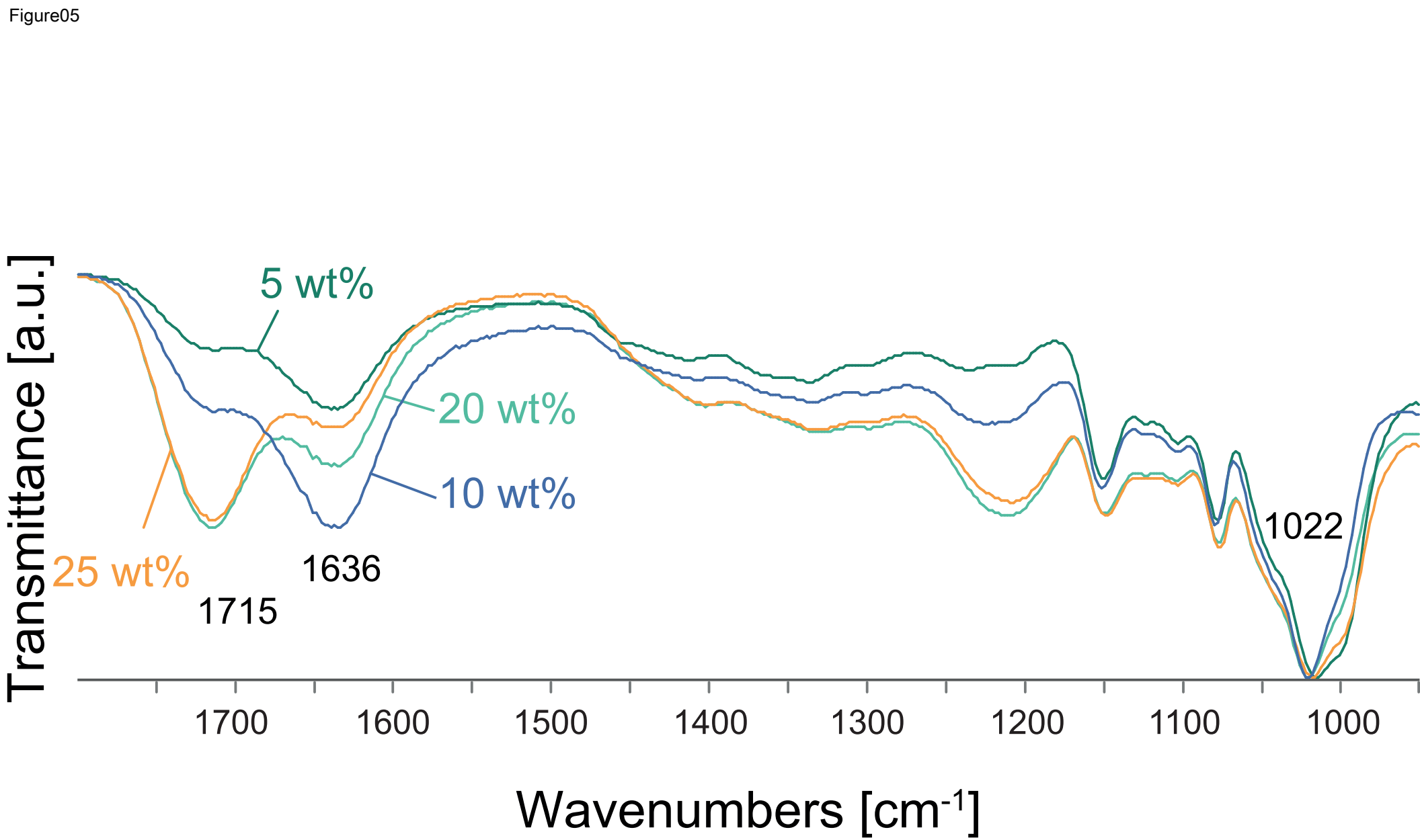
Transmittance [a.u.]
5 wt%
20 wt%
10 wt%
25 wt%
1715
1636
1022
1700
1600
1500
1400
1300
1200
1100
1000
Wavenumbers [cm-1]

Figure06

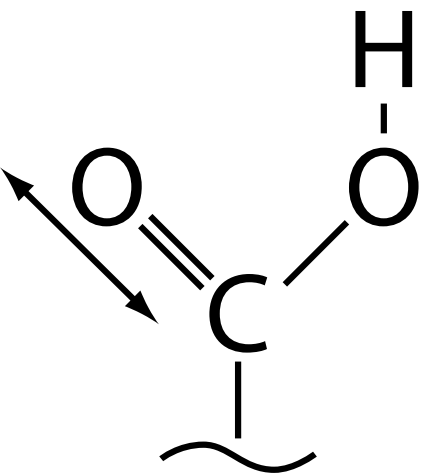

$\nu_{C=O}$

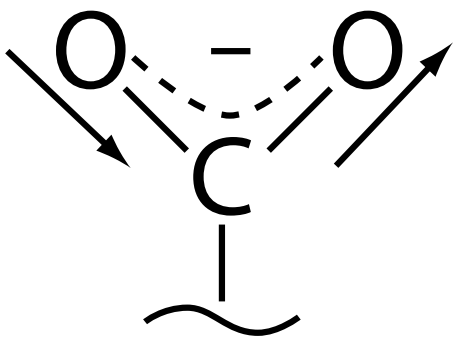

ν_{as}

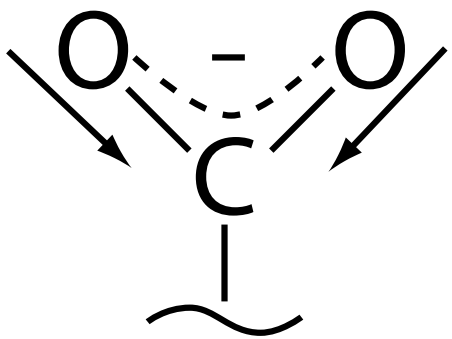

ν_{s}

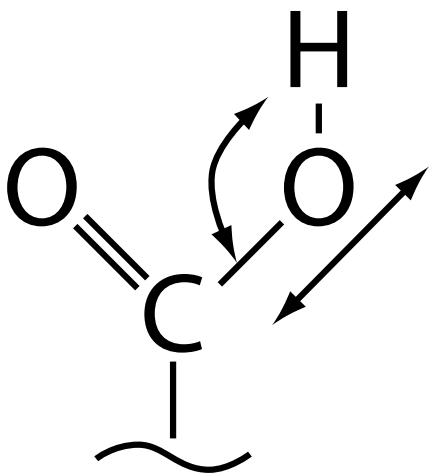

$\nu_{C\text{-}OH}$

Figure07

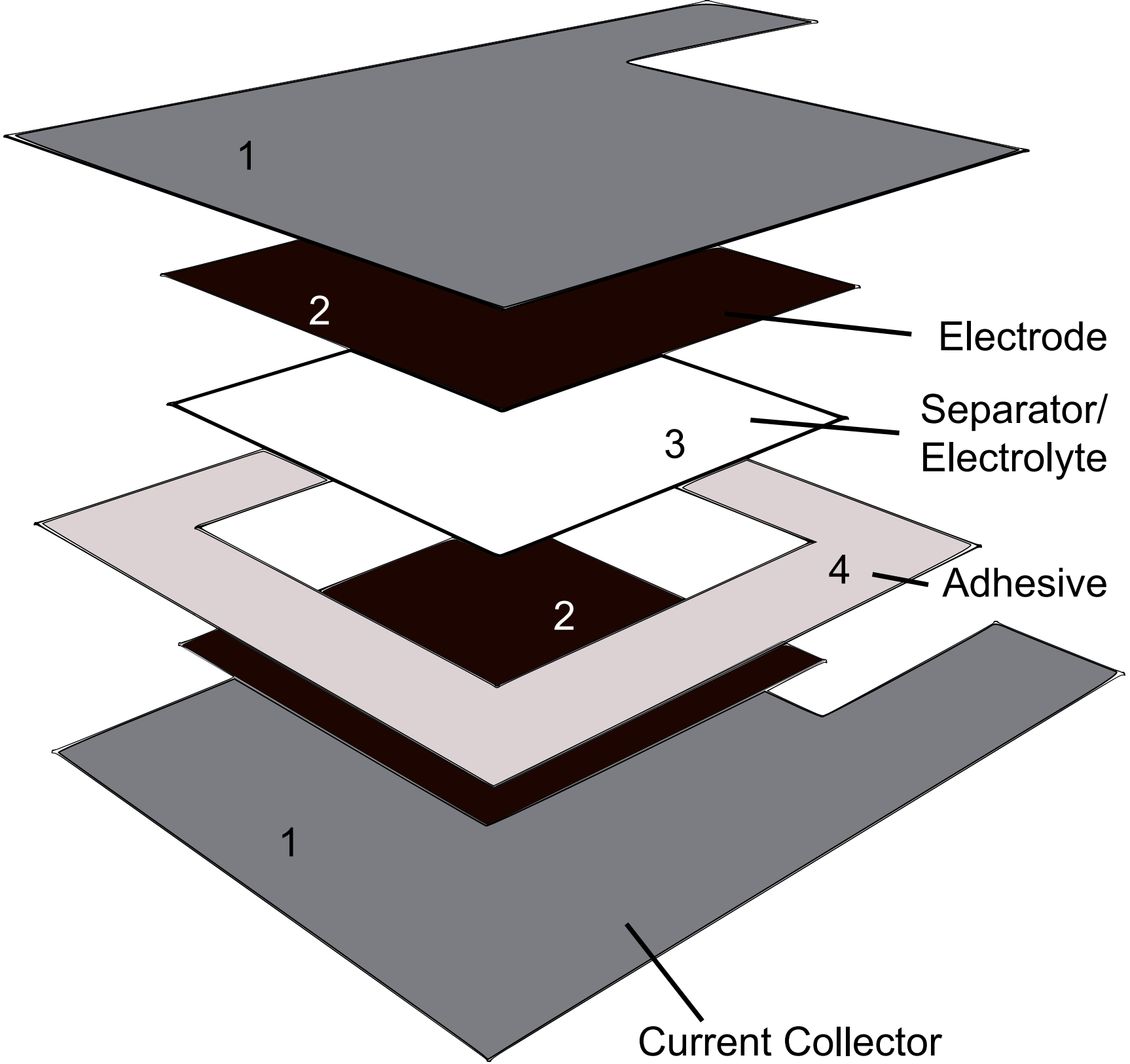
1
2
Electrode
Separator/
Electrolyte
3
4
Adhesive
2
1
Current Collector

Figure08

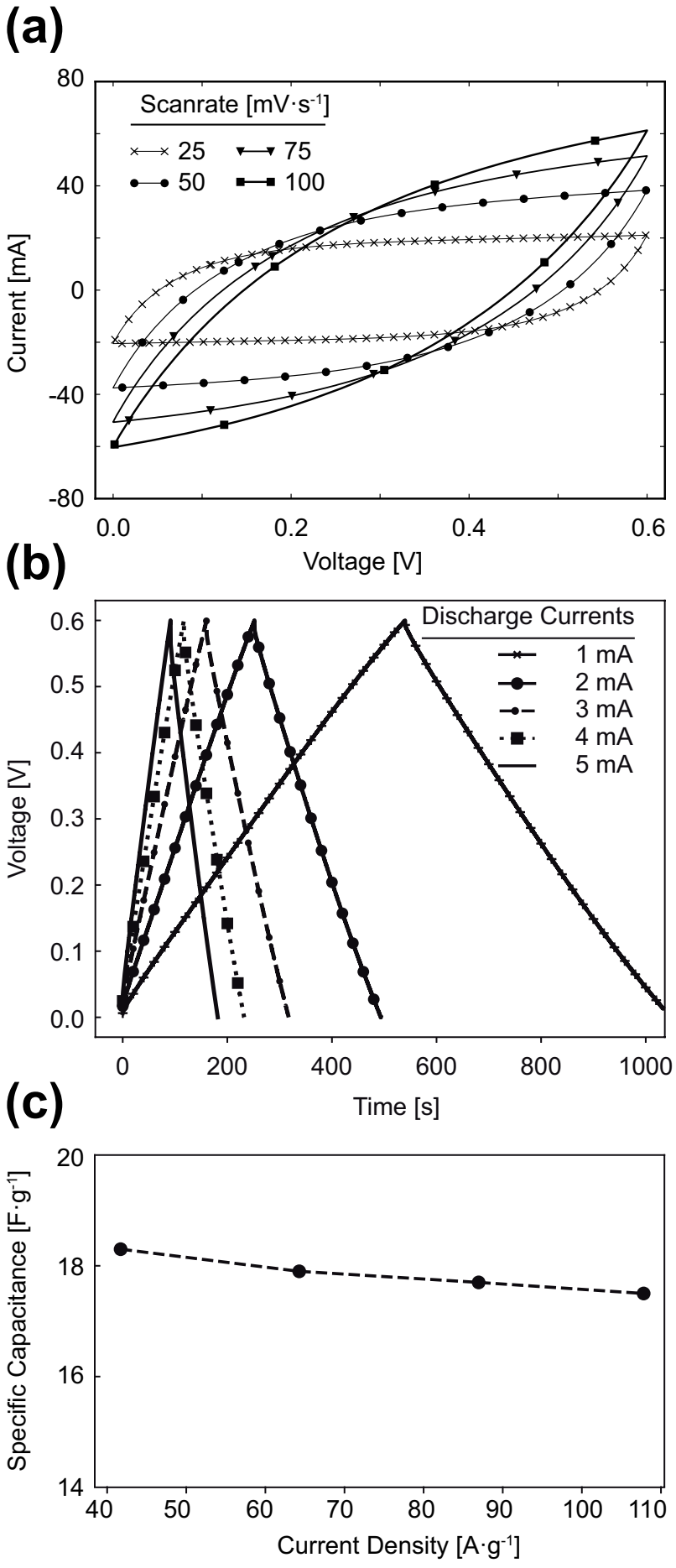
(a)
Scanrate [mV·s-1]
25
75
50
100
Current [mA]
Voltage [V]
(b)
Discharge Currents
1 mA
2 mA
3 mA
4 mA
5 mA
Voltage [V]
Time [s]
(c)
Specific Capacitance [F·g-1]
Current Density [A·g-1]

Figure09

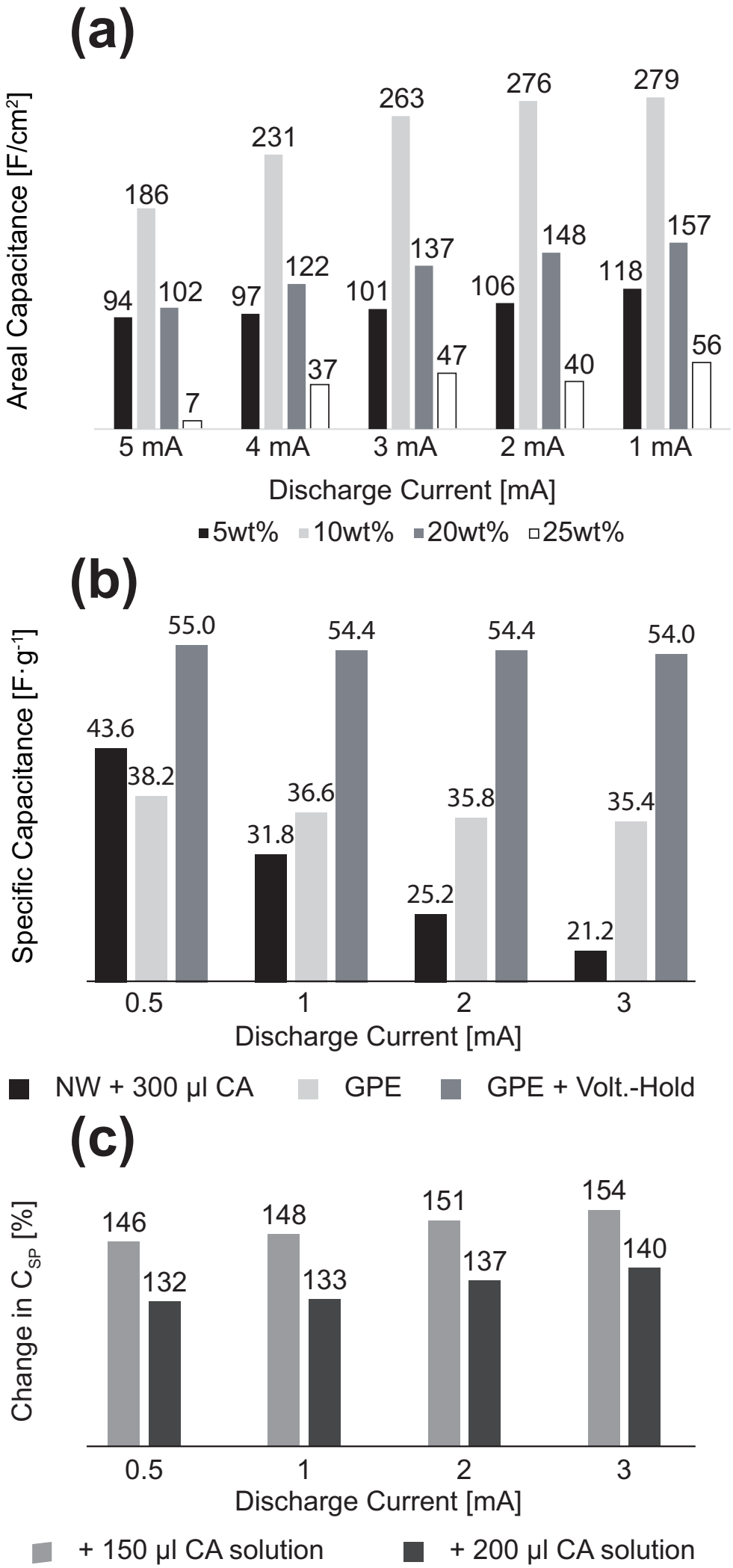
(a)
Areal Capacitance [F/cm²]
94
186
102
7
97
231
122
37
101
263
137
47
106
276
148
40
118
279
157
56
5 mA
4 mA
3 mA
2 mA
1 mA
Discharge Current [mA]
5wt%
10wt%
20wt%
25wt%
(b)
Specific Capacitance [F·g⁻¹]
43.6
38.2
55.0
31.8
36.6
54.4
25.2
35.8
54.4
21.2
35.4
54.0
0.5
1
2
3
Discharge Current [mA]
NW + 300 µl CA
GPE
GPE + Volt.-Hold
(c)
Change in C_SP [%]
146
132
148
133
151
137
154
140
0.5
1
2
3
Discharge Current [mA]
+ 150 µl CA solution
+ 200 µl CA solution

Table01

Table 1: Preparation of hydrogels with different CA concentrations at constant starch fraction at 30 wt%.

Mixing Ratio TPS:H_2O-ST	CA wt% (rounded figure)	H_2O wt%	Conductivity [$mS \cdot cm^{-1}$]	Viscosity [$Pa \cdot S$] at 100 s^{-1}
1:1	25	45	1.11 ± 0.18	1.7 ± 0.1
1:1.5	20	50	2.02 ± 0.06	3.3 ± 0.1
1:4	10	60	2.30 ± 0.07	16.0 ± 0.4
1:10	5	65	1.64 ± 0.01	20.3 ± 1.6

Table02

Table 2: Formulation of activated carbon based electrode ink.

Active material	Conductive additive	Binder	Solvent
29 wt%	2 wt%	20 wt%	49 wt%
Activated Carbon NORIT A SUPRA EUR	Carbon-Black Vulcan XC-72R		Distilled Water

Table03

Table 3: Formulation of activated carbon based electrode ink.

Active material	Conductive additive	Binder	Solvent
29 wt%	2 wt%	20 wt%	49 wt%
Activated Carbon NORIT A SUPRA EUR	Carbon-Black Vulcan XC-72R		Distilled Water

Table04

Table 4: Characteristics of printed supercapacitors reported elsewhere.

Electrode	Electrolyte/ Separator	Process	Csp [F/g]	Csp [F/cm2]	Reference	Year
Activated Carbon (AC) + Graphite	LiCl/PEO, THF	Screen Printing	21* (GCD)	4 cm^2: 166 mF, 6 cm^2: 295 mF	[42]	2017
Graphene	PVA-H_2SO_4	Screen Printing	190 (GCD)		[43]	2017
AC+Chitosan + Acetic Acid + H_2O	NaCl 1.5M·l^{-1}, Gelatin/Starch	Blade-Coating	20 (CV)	10.5 cm^2	[14]	2017
AC+Chitosan + Acetic Acid + H_2O	NaCl, paper	Screen Printing	20**		[44]	2017
Carbon Black (CB)	KOH, PVA	Litho-/Flexographic		0.72 and 4 mF·cm^{-2}	[45]	2015
AC + CB + Poly(vinyl alcohol-co-ethylene) + DMSO + additive	ammonium salt, PVA + H_2O	Spray coating	10.6	71.8 mF·cm^{-2}	[46]	2015
AC + Carboxymethylcellulose, H_2O	Nippon TF4050	Blade-coating	26*	4 cm^2: 450 mF, 2 cm^2:210 mF	[47]	2014

* total AC (activated carbon) mass only; **total dry ink AC mass

Supplementary Information

1 Preparation of Hydrogels

Preliminary investigations have provided insights into the problems of starch-based hydrogels, particularly retrogradation and susceptibility to mould infestation. In order to prevent the latter, a suitable substance was found in citric acid, which is both a widely used preservative in the food industry and a reaction partner for starch modification. Crosslinking of starch with citric acid was already reported [1]. Previous tests have confirmed the conclusion of Reddy et al. that the process time is critical. A prolonged thermal load during processing of cornstarch and citric acid negatively affects the properties of the thermoplastic starch, i.e. hydrogels made from these thermoplastic starches were very sticky and difficult to process in screen printing. For the controlled processing of citric acid and cornstarch, extrusion and melt-blending were considered. Since sophisticated machines and profound process knowledge are required for extrusion, the simpler melt-blending method using a laboratory hot plate was used for the examination of thermoplastic starch powders.

Three different methods for hydrogel preparation were tested. The ultrasound treatment showed consistent results and homogenous hydrogels. Additionally, ultrasonic treatment provided the fastest processing time amongst the other methods microwave oven and a hotplate with magnetic stirrer.

The process of ultrasonic treatment starts with mixing melt-blended citric acid-cornstarch powder with a cornstarch water suspension. The horn of the ultrasound processor is immersed directly into the mixture. Cycle is set to 100 %. The duration of the treatment depends on the ratios of the materials and the volume of the sample. The end of the process is indicated by a spontaneously drop in sound and applied power due to the increase in viscosity. It is an inherent problem of the direct ultrasound processing, that the material in the vincinity of the horn experiences the highest impact. As such, the viscosity is not homogenously distributed through the whole sample. This can be seen in the viscosity measurements shortly after processing and after the first 24 hours, when the viscosity has stabilised.

2 FTIR Measurements Extrusion and Melt-Blending

Initially, starch filament was prepared via extrusion with Coperion ZSK 18 double screw extruder (Stuttgart, Germany). The extruder barrel length to diameter ratio was 41. The extruder screw was made of conveying, kneading and mixing elements. The design of the screw is intellectual property of “Institut für Kunststofftechnik”, Stuttgart University, where the tests were performed. In contrast to other reports [2–5], only cornstarch and citric acid was used for extrusion without any further chemical as plasticizer, e.g. water or glycerol. The extruder suggests better control over the parameter setting. However, the process volume is rather high, requiring at least 500 g per test run, even with a “small” laboratory extruder. With the first test run it was obvious, that extrusion requires a deep knowledge about processing parameters. Hence, a much simpler and vastly available process was found in using a laboratory hotplate for melt blending. The FTIR-analysis of the powders obtained from both extrusion and hotplate melt-blending was supposed to identify structural differences. As indicated by Figure 1, the difference is not very pronounced, so that melt-blending on the hot plate was pursued.

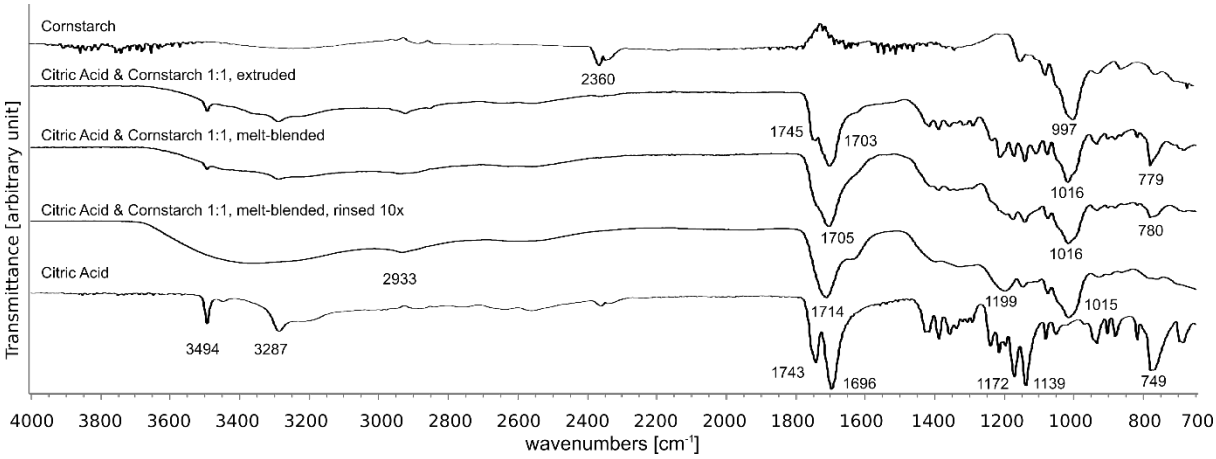

Figure 1: FTIR-Spectra of powder materials.

The FTIR spectrum of citric acid cornstarch (1CA1ST) blend exhibits characteristic signals deriving from both components. The broad dip in the region of 1790 and 1500 cm^{-1} is referring to the C=O bond [6] and represents a typical region of carboxylic acids (or esther groups). The two separate absorption peaks at 1696 and 1743 cm^{-1} in pure CA indicating C=O stretching correspond to free and hydrogen bonded carboxyl groups [7]. In the melt blended thermoplastic starch (TPS) powder the two peaks merge to one strong peak at 1714 cm^{-1}. This dip representing carbonyl-group region (1700-1725 cm^{-1}) is characteristic for carboxylic acids. The absorbance peak at 997 cm^{-1} in cornstarch is appearing in the composite with a light shift to 1020 cm^{-1}. This band refers to C–O–C stretching in the anhydroglucose ring [2]. The very broad absorption band in the functional group region between 2300 and 3600 cm^{-1} can be attributed to characteristic O-H stretching of carboxyl groups [8]. As reported by [9], broadening of the peak in the range 2500-3500 cm^{-1} is due to the OH groups in citric acid. In the spectrum of CA powder, C=O stretching of free and hydrogen bonded carboxyl groups (Doll et al. 2006) is shown at 1743 cm^{-1}, an indication for aliphatic carboxylic acids (Garcia et al. 2011). The excess of CA is also represented as a miniscule absorbance peak in the spectrum of extruded starch (1CA1ST - extruded). Although less pronounced, it is also observable in the hotplate melt-blended TPS (1CA1ST). With rinsing the powder prior to the measurements, the free i.e. unreacted CA is removed, as discussed elsewhere [10]. The rinsed 1CA1ST reveals a broadened peak at 1714 cm^{-1} and additionally an absorbance shoulder at 1636 cm^{-1}. According to [11] this band can be ascribed to water adsorbed in the amorphous region of starch granules. The intensity of the band decreases by increasing crystallinity of starch [12]. The rinsed 1CA1ST shows a shoulder at 1636 cm^{-1}, which may be attributed to water uptake while rinsing and hence reduction in crystallinity.

3 Rheological Measurements

3.1 Viscosity Change with Hydrogel Aging

The shape of the viscosity plots, indicated by the curve in Figure 2c, clearly showed that the measurement time is sufficient to approximate a stable value that has changed only slightly in the last third of the 300 seconds covered by the measurement period. The shape additionally indicates that the gels are shear thinning fluids, since the viscosity drops at the beginning of the measurement, but stabilizes roughly after half the measurement time

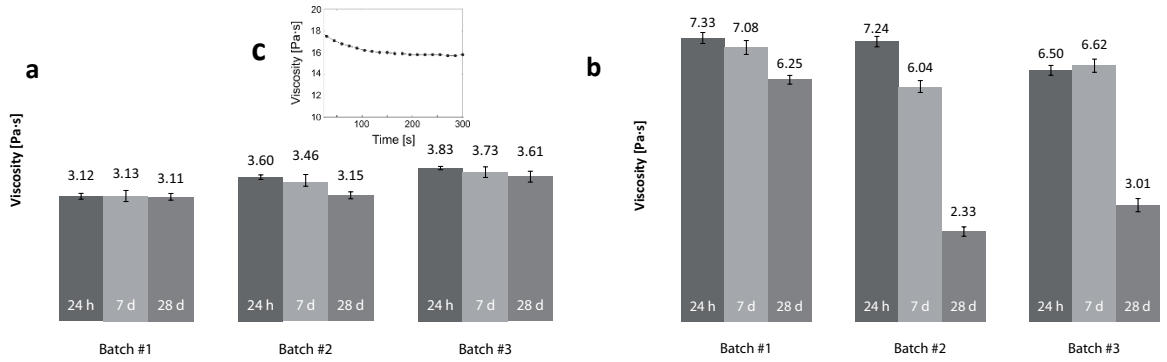

Figure 2: Change in viscosity over indicates good stability of the CA modified cornstarch hydrogel (a). Physically modified cornstarch hydrogel (b) shows a higher reduction in viscosity while aging. (c) indicates the progress of viscosity values during measurement.

Figure 2a shows a slight change in the viscosity of the starch modified with citric acid over a period of 27 days. In view of the fact that cornstarch is a natural product with variations in its quality, this small change is negligible. In Figure 3b the change in viscosity of physically modified cornstarch is shown. The higher initial viscosity indicates the stiffer gel structure of this gel. It is also obvious from Batch#2 and Batch#3 that structural modification takes place, indicated by the huge viscosity drop between 7 and 28 days sample life. In addition, almost all samples showed a beginning mould growth already after one week. This was not observed with citric acid modified cornstarch hydrogels, or only after a much longer period of time. Storing the gel in the refrigerator at temperatures around 8 °C slows down the formation of mould, but the structure of the gel also changes as a result. No measurements were carried out in this respect, but even when the gel was stirred before application in screen printing, the experimenter experienced a subjectively perceived change in the flow behaviour and the gel texture.
Three kinds of water are assumed to be existent in hydrogels: tightly or loosely bound and free water [13–15]. Syneresis is the tendency of gels to release spontaneously small volumes of the loosely bound liquid [16], an effect that is accompanied by retrogradation [17,18]. Retrogradation begins in the interfacial regions between hydrogel and surrounding atmosphere. The surface gets crusty while inside it stays gel-like. Eventually, the crystalline parts expand and penetrate into the gel until it hardens completely. Retrogradation and water loss lead to increase in viscosity. Nevertheless, almost all samples show the tendency of decreasing viscosity. Figure 2 shows the viscosity change over a three-week period. The CA modified cornstarch is rather stable, indicating a less pronounced retrogradation. The slight reduction in viscosity may result from the pH value of the citric acid, which is about 2. It can promote the hydrolysis of starch, as many starch grains are destroyed or glucose chains are hydrolyzed due to the acid pH-level [19]. According to Hirashima et al., large amounts of citric acid lead to the rupture of starch granules. Since the gels are not pH-neutral after ultrasonic sonication, acid hydrolysis can progress over time. Overall, the achieved viscosity ranges are suitable for screen printing.

The end of gelation was indicated by the power drop of the ultrasound processor, which was accompanied by a drastic increase in the viscosity of the gel that was then formed. Locally around the tip of the sonotrode horn the viscosity increases earlier than in the surrounding area and thus the process may terminate prior to gelling the complete suspension available in the container. In case of a larger suspension volume, this leaves a rather high fraction of the water-starch-TPSP suspension unreacted. If the volume is small, a higher fraction of the suspension is actually gelled. The non-gelled suspension reduces the viscosity of the hydrogel during the first 24 hours due to diffusion. For long-term rheological measurements, larger amounts of hydrogel were produced than for the evaluation of the ionic conductivity of different citric acid contents in the hydrogels. This explains different initial values of viscosity in the same formulation.

3.2 Thixotropy Measurements

Another important characteristic for printing inks is thixotropy, which is the time depending recovery of viscosity after shearing. A very thixotropic fluid needs more time for regaining the inner structure and build up viscosity. Evaluating the recovery phase facilitates prediction on the levelling behaviour. A smooth ink layer surface can be expected from a rather long recovery period and a more structured surface from fast recovery but in turn, this leads to a sharper edge of the printed image. It is not necessary that the initial viscosity be reached again. The Three Interval Thixotropy Test (3ITT) [29] is used to gain information about the behaviour of the liquid while being processed e.g. in printing applications. This test is superior to the often-referred hysteresis test, which is not very accurate, since the inks rheological history is unknown [20].

With 3ITT, the sample is subject to a defined low impact shearing prior to a drastic stress, followed by a relaxation step for monitoring recovery of the fluid. All hydrogels show fast recovery of viscosity and thus low thixotropy. The gel structure is recovered at once. Consequently, there is no levelling, hence a structured surface is the result. If the printed hydrogel layer is used as a separator in either printed batteries or supercapacitors, the surface quality is of minor importance, since a rugged electrode surface is pressed onto the separator surface. It is rather important for the property as separator that the printed hydrogel layer retains a certain moisture content and that it is possible to penetrate the pores of the electrode layer when the components are assembled.

3.3 Loss Factor and Flow Curve

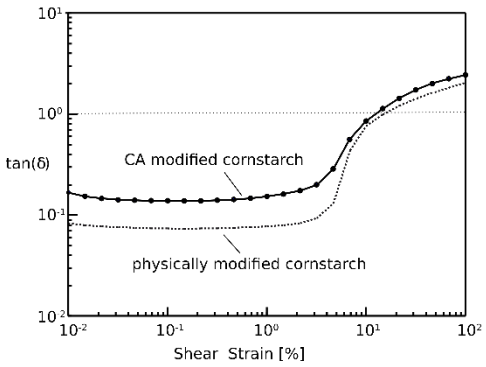

Figure 4: Loss factor and flow point of physically and chemically modified cornstarch hydrogels.

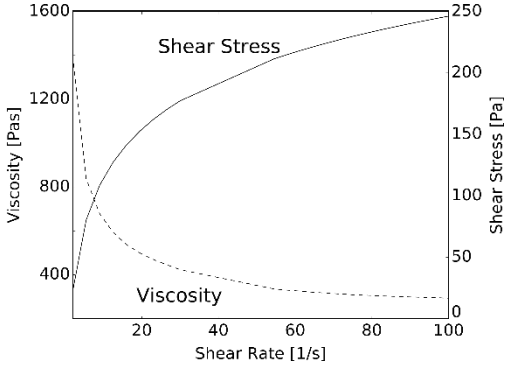

Figure 5: Flow curve of chemically modified cornstarch hydrogel.

The loss factor of the physically and the chemically modified hydrogel displayed by Figure 4 shows gel structure, i.e. $\tan(\delta) < 1$, over a wide range of shear strain. Both samples begin to flow at the same shear strain of around 10%, when $\tan(\delta) = 1$.

The flow curve depicted by Figure 5 indicates Casson fluid characteristic by the shifted origin of the shear stress. The hydrogel displays infinite viscosity at zero rate of shear, a yield stress below which no flow occurs and a zero viscosity at an infinite rate of shear [21]. The reduction of viscosity by increasing the shear rate points to pseudoplasticity.

4 Microscope Analysis

Microscope images were taken with an alicona infinite focus system. The microscope is capable of creating three-dimensional images using focus variation [31]. However, the analysis of dry hydrogel layers was performed using two-dimensional images at 5x, 10x, 20x, and 50x magnification. However, due to the small focal depth, the sharpness of the image may reveal an impression of the topography.

The optical analysis of the dry hydrogel layer provides information on the structural properties of the different formulations. As the CA proportion increases, a smoother film is formed, indicated by the depth of focus of the individual image areas. At 5 wt% CA (a) many areas are not in focus. This is due to larger associated structures. At 10 wt% (b) the area of focus is larger. The characteristic ghost granules show in both cases that water is incorporated into starch. The gel film in (b) is more homogeneous than in (a). With the further increase of the CA percentage, the proportion of ghost granules is reduced. At 25 wt% (d) none of these are visible. The reason is assumed to be acid hydrolysis, which depends on the CA content. With increasing acid hydrolysis, also viscosity of the gel is reduced, as shown in Table 1.

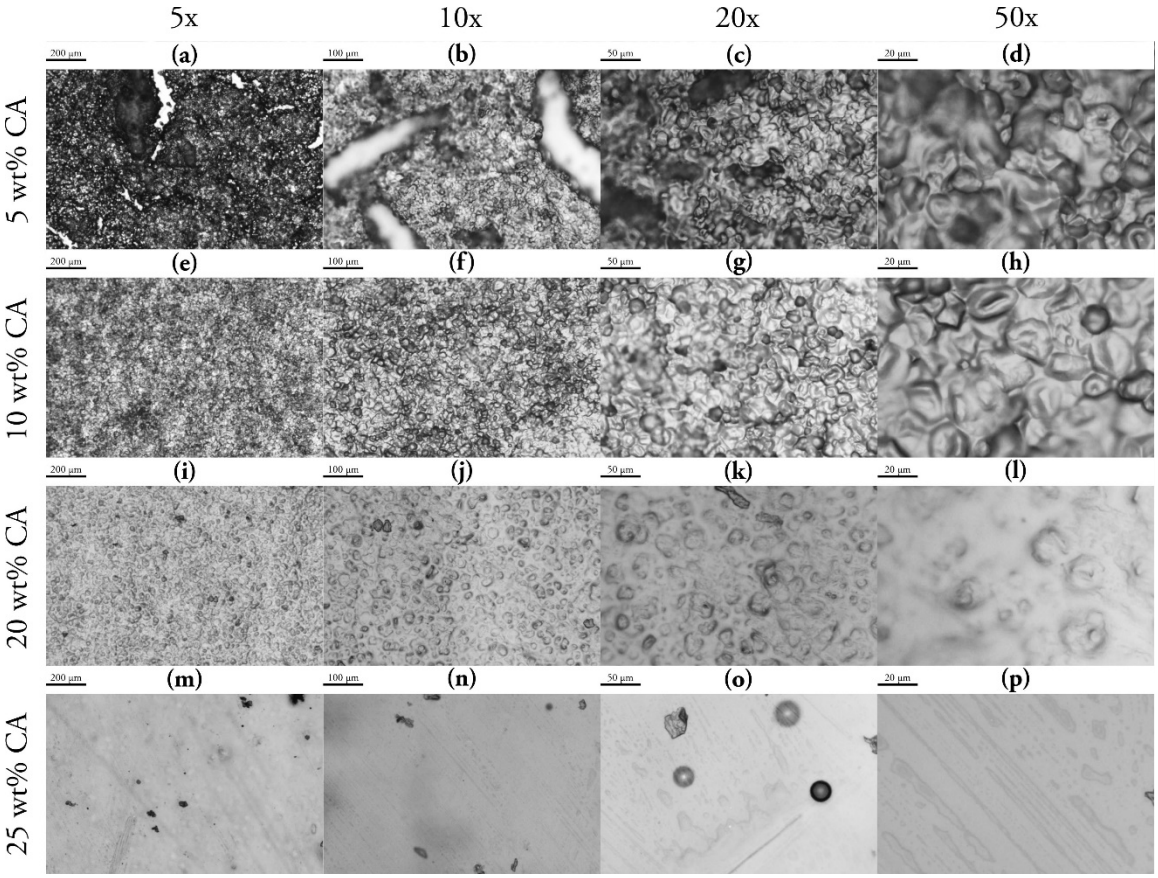

Figure 6: Microscope images of dry hydrogel layers. (a)-(d) 5 wt%, (e)-(h) 10 wt%, (i)-(l) 20 wt%, (m)-(p) 25 wt%. The appearance of starch granules indicate low acid hydrolysis. With higher acid content, the granules are destroyed, the ink film is highly transparent and smooth.

In the first row of Figure 6 the lowest CA concentration of 5 wt% is shown. This hydrogel provides swollen starch granules. It is more than likely that the small proportion of CA allows only some hydrolysis and that the starch grains therefore remain unaffected. The gel forms very uneven surfaces, which even cannot be captured by low magnification focal-depth. With the 50x magnification only small parts of the image are in focus.

In the second row the hydrogel containing 10 wt% CA shows a huge coverage of largely swollen starch granules, which may be interpreted as absorbed water. This corresponds with the FTIR peak at 1636 cm^{-1}, which is pronounced with this hydrogel. From the 20x and 50x magnifications shown in Figure 6 (g) and (h), it can be seen that some parts of the images are not covered by the focal depth of the microscope lens, indicating a rough surface topography. This can result from the longer polymer chains, which form larger domains and can also be seen from the higher viscosity.

In the third row, the hydrogel containing 20 wt% CA displays some observable starch granules. The darker shaded particles seem to be less swollen and more intact than die brighter ones. Especially in the 50x magnification it can be seen that there are some ghost granules, but

the distance between the single granules is rather large. The 5x and 10x magnifications provide information about the homogeneity of the layer and the rather small topological differences in the entire test area, which can be deduced from only small out-of-focus parts.

The highest CA concentration of 25wt% is shown in the fourth row. At first glance, there are no starch granules visible. However, with a closer look at the 5x magnification, the round shaped bright shaded parts in the image may be assumed to represent starch particles or agglomerates. The combination of ultrasound treatment and citric acid facilitates hydrolysis, which is also a time-dependent process. It is assumed that 3 different stages occur: the first is the rapid attack of the outer parts of the starch grain. Then the destruction of the inner structure and finally the breaking open of the crystalline structure from the inner starch parts.

In Figure 6 (p), the residuals of the gelatinized starch parts may be seen, smeared by the application process (doctor blade coating). Some structures resemble starch granule ghosts known from starch gelatinisation. The 25 wt% CA containing hydrogel forms a uniform, very transparent ink film. Only entrapped bubbles and occasionally residual corn granules can be noticed, as seen in the 20x magnification image, see Figure 6 (o).

The microscope images support the hypothesis that excess CA forces the hydrolysis of the starch, since no or very few starch granules are present.

5 Layout of the Printed Supercapcitors

In this work two different layouts were used for characterisation of printed supercapacitors, differing mostly in size of the active area, but also the way the separator is applied to the electrodes. The smaller layout is shown in Figure 7. This setup provides an active area of 1 cm^2. The separator is applied by doctor-blading in the cavity formed by insulating layer or the adhesive foil respectively. This procedure was reasonable for preliminary tests and fast evaluation of parameters, since the specimen could be assembled and tested very quickly. The insulating layer can be made of UV-light crosslinking inks Ultrapack UVC or UVLEDC from Marabu GmbH & Co. KG (Tamm, Germany). The insulating UV-ink layer provides the well-defined active area. It also determines the thickness and volume of the separator. This printed layer was in the progress of the experiments substituted by a 260 µm thick double-side adhesive tape, providing strong adhesion between the supercap-strips and simplified assembly of the device. The hydrogel separator ink is the last layer, which is applied into the cavity formed by UV-ink layer or alternatively adhesive tape. Two strips of the multilayer composite attached face-to-face form the supercapacitor.

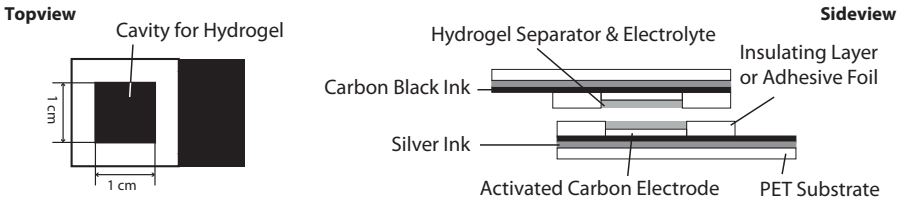

Figure 7: Schematic illustration of the printed supercapacitor arrangement.

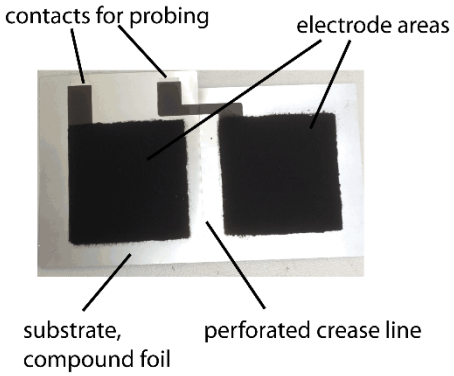

Figure 8: Coplanar design of the printed supercapacitor on compound substrate. The perforated line between the electrode areas facilitates folding of one electrode on top of the other.

Different printing designs were used in subsequent tests. The electrodes were printed on a coplanar current collector made of silver ink coated with a layer of chemically more stable carbon black. The mass of the electrodes was determined by means of a precise laboratory scale. The hydrogel was applied by screen or stencil printing, depending on the adhesion of the electrode layer to the carbon black current collector. If an ink formulation containing very only a small amount of binder is used, paste adhesion is very low. When the electrode surface is being printed with the hydrogel separator, the electrode can detach from the underlying layer due to ink splitting and thus render the device unusable. In this case, however, it is possible to use stencil printing instead of screen printing. After applying the hydrogel separator, a water dispersion adhesive was applied with cotton sticks. The adhesive layer can also be printed. However, since only a small number of supercapacitors were characterized, manual adhesive application was more reasonable. When all layers have been applied, the right electrode is folded down onto the left electrode. A perforation line between the electrodes facilitates this assembly step.

The electrode ink made of activated carbon, conductive additive and PEDOT:PSS (PH1000) had poor adhesion, which is why stencil printing was preferred.

6 Electrochemical Characterisation

Several electrochemical measurement methods allow for characterisation of the supercapacitor devices. The most often reported value is the gravimetric specific capacitance in Farad per gram [F g^{-1}] related to the active material. However, determination of the capacitance is not as straightforward as it sometimes is presented. In [22] the authors discuss the validity of calculated specific capacitance in scientific publications. Cyclic Voltammetry (CV) data allow for determination of the capacity of the supercapacitor, but the shape of the voltammogram can influence the quality of the calculations, especially if the shape of the curve is very different from the ideal case of a rectangle. Additionally, the chosen segment of voltammogram influences the result [23]. Capacitance determination from CV depends on a myriad of parameters [24]. For instance, temperature influences capacitance determination [25].

Many approaches and formulas for calculating specific capacity are discussed in scientific articles [23,26–28]. Foremost, when faradaic processes are present, the calculation or estimation of the capacitance is rather difficult.

6.1 Ionic Conductivity Tester

Two opposing stainless steel electrodes with an area of 7.5 cm^2 in a 3D-printed measurement setup were used to determine the ionic conductivity. In order to achieve meaningful results, a certain ratio of electrode surface to layer thickness of the gel electrolyte must be given [30]. The 3D-printed measuring set-up allows the adjustment of a reproducible contact pressure by means of two screws. The hydrogel electrolyte was applied with a defined layer thickness of 360 µm using a squeegee process and a mask made of a sheet of plastic.

When applying the gels, it was ensured that there were no air inclusions or defects in the gel layer. The intercept of the data curve with the x-axis of the Nyquist Impedance plot marks the ionic resistance of the specimen under test.

The intercept of the Nyquist plot with the x-axis representing the real part of the impedance indicates the ionic conductivity. The corresponding values were obtained by manual extraction of the data from the Nyquist plots shown in Figure 10.

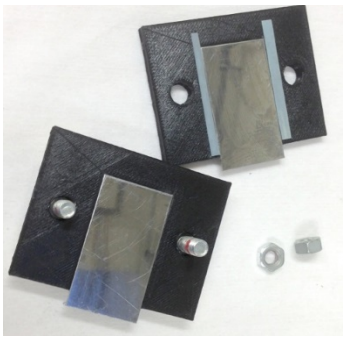

Figure 9: Test setup for characterising the ionic conductivity of the solid electrolyte.

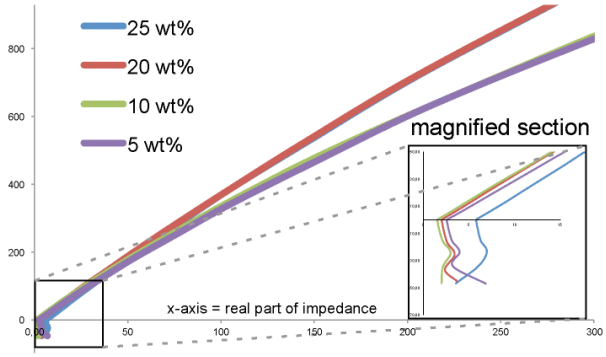

Figure 10: Excerpting the resistance values from the Nyquist impedance plot.

References

[1] Reddy N, Yang Y. Citric acid cross-linking of starch films. Food Chemistry 2010;118(3):702–11.

[2] Olivato JB, Grossmann M, Yamashita F, Eiras D, Pessan LA. Citric acid and maleic anhydride as compatibilizers in starch/poly(butylene adipate-co-terephthalate) blends by one-step reactive extrusion. Carbohydrate Polymers 2012;87(4):2614–8.

[3] Pushpadass HA, Kumar A, Jackson DS, Wehling RL, Dumais JJ, Hanna MA. Macromolecular Changes in Extruded Starch-Films Plasticized with Glycerol, Water and Stearic Acid. Starch - Stärke 2009;61(5):256–66.

[4] Jiugao Y, Ning W, Xiaofei M. The Effects of Citric Acid on the Properties of Thermoplastic Starch Plasticized by Glycerol. Starch - Stärke 2005;57(10):494–504.

[5] Antonio J.F. Carvalho, Marcia D. Zambon, A. Aprigio da Silva Curvelo, Alessandro Gandini. Thermoplastic starch modification during melt processing: Hydrolysis catalyzed by carboxylic acids. Carbohydrate Polymers 2005(62):387–90.

[6] Cruz LCd, Miranda CSd, Santos WJd, Gonçalves APB, Oliveira JCd, José NM. Development of Starch Biofilms Using Different Carboxylic Acids as Plasticizers. Mat. Res. 2015;18:297–301.

[7] Doll KM, Shogren RL, Willett JL, Swift G. Solvent-free polymerization of citric acid andD-sorbitol. J. Polym. Sci. A Polym. Chem. 2006;44(14):4259–67.

[8] Bin-Dahman OA, Jose J, Al-Harthi MA. Compatibility of poly(acrylic acid)/starch blends. Starch - Stärke 2015;67(11-12):1061–9.

[9] Cui Z, Beach ES, Anastas PT. Modification of chitosan films with environmentally benign reagents for increased water resistance. Green Chemistry Letters and Reviews 2011;4(1):35–40.

[10] Shi R, Bi J, Zhang Z, Zhu A, Chen D, Zhou X et al. The effect of citric acid on the structural properties and cytotoxicity of the polyvinyl alcohol/starch films when molding at high temperature. Carbohydrate Polymers 2008;74(4):763–70.

[11] Kizil R, Irudayaraj J, Seetharaman K. Characterization of irradiated starches by using FT-Raman and FTIR spectroscopy. J Agric Food Chem 2002;50(14):3912–8.

[12] Nagaraj P, Sasidharan A, David V, Sambandam A. Effect of Cross-Linking on the Performances of Starch-Based Biopolymer as Gel Electrolyte for Dye-Sensitized Solar Cell Applications. Polymers 2017;9(12):667.
[13] Tranoudis I, Efron N. Water properties of soft contact lens materials. Cont Lens Anterior Eye 2004;27(4):193–208.
[14] Krystofiak K, Szyczewski A. Study of dehydration and water states in new and worn soft contact lens materials. Optica Applicata 2014;44(2):237–50.
[15] Pasqui D, Cagna M de, Barbucci R. Polysaccharide-Based Hydrogels: The Key Role of Water in Affecting Mechanical Properties. Polymers 2012;4(4):1517–34.
[16] Walter RH, Taylor S. Polysaccharide Dispersions: Chemistry and Technology in Food. 1st ed. s.l.: Elsevier professional; 1997.
[17] Tako M, Tamaki Y, Teruya T, Takeda Y. The Principles of Starch Gelatinization and Retrogradation. FNS 2014;05(03):280–91.
[18] Wang S, Li C, Copeland L, Niu Q, Wang S. Starch Retrogradation: A Comprehensive Review. Comprehensive Reviews in Food Science and Food Safety 2015;14(5):568–85.
[19] Hirashima M, Takahashi R, Nishinari K. Effects of citric acid on the viscoelasticity of cornstarch pastes. J Agric Food Chem 2004;52(10):2929–33.
[20] Howard A. Barnes. Thixotropy - a review. Journal of Non-Newtonian Fluid Mechanics 1997;70:1–33.
[21] Dervisoglu M, Kokini JL. Steady Shear Rheology and Fluid Mechanics of Four Semi-Solid Foods. J Food Science 1986;51(3):541–6.
[22] G. A. Ragoisha, Y. M. Aniskevich. False capacitance of supercapacitors. Minsk; 2016.
[23] Kampouris DK, Ji X, Randviir EP, Banks CE. A new approach for the improved interpretation of capacitance measurements for materials utilised in energy storage. RSC Adv 2015;5(17):12782–91.
[24] Gamry Instruments. Testing Super-Capacitors Part 1: CV, EIS, and Leakage Current. Application Note. Warminster PA, USA.
[25] H. Gualous, Kauffmann JM, Bouquain D, Berthon A. Thermal study of supercapacitor serial resistance. Lausanne, Switzerland; 2002.
[26] P. Kurzweil, B. Frenzel, R. Gallay. Capacitance Characterization Methods and Ageing Behaviour of Supercapacitors. Deerfield Beach, FL., U.S.A.
[27] Ban S, Zhang J, Zhang L, Tsay K, Song D, Zou X. Charging and discharging electrochemical supercapacitors in the presence of both parallel leakage process and electrochemical decomposition of solvent. Electrochimica Acta 2013;90:542–9.
[28] Lungoci C, Danut OI. About Supercapacitors Parameters Determination. Bulletin of the Transilvania University of Braşov 2009;2(51):279–86.
[29] Toker OS, Karasu S, Yilmaz MT, Karaman S. Three interval thixotropy test (3ITT) in food applications: A novel technique to determine structural regeneration of mayonnaise under different shear conditions. Food Research International 2015;70:125–33.
[30] Railanmaa A, Lehtimäki S, Lupo D. Comparison of starch and gelatin hydrogels for non-toxic supercapacitor electrolytes. Appl. Phys. A 2017;123(6):42.
[31] Alicona Imaging GmbH. Focus-Variation: The technical principle. [September 04, 2018]; Available from: https://www.alicona.com/focus-variation/.